EFFECT OF DIFFERENT TYPES OF STATIC MIXER GEOMETRY ON QUALITY OF MICROBUBBLE GENERATION

TEE WU YANG

FACULTY OF ENGINEERING
UNIVERSITY OF MALAYA
KUALA LUMPUR

2020

EFFECT OF DIFFERENT TYPES OF STATIC MIXER GEOMETRY ON QUALITY OF MICROBUBBLE GENERATION

TEE WU YANG

THESIS SUBMITTED IN FULFILMENT OF THE REQUIREMENTS FOR THE DEGREE OF MASTER OF MECHANICAL ENGINEERING

FACULTY OF ENGINEERING
UNIVERSITY OF MALAYA
KUALA LUMPUR

2020

UNIVERSITY OF MALAYA

ORIGINAL LITERARY WORK DECLARATION

Name of Candidate: Tee Wu Yang

Matric No: KQK180027

Name of Degree: Master of Mechanical Engineering

Title of Research Report: Effect of Different Types of Static Mixer Geometry on Quality Microbubble Generation

Field of Study: Fluid Mechanics

I do solemnly and sincerely declare that:

(1) I am the sole author/writer of this Work;
(2) This Work is original;
(3) Any use of any work in which copyright exists was done by way of fair dealing and for permitted purposes and any excerpt or extract from, or reference to or reproduction of any copyright work has been disclosed expressly and sufficiently and the title of the Work and its authorship have been acknowledged in this Work;
(4) I do not have any actual knowledge nor do I ought reasonably to know that the making of this work constitutes an infringement of any copyright work;
(5) I hereby assign all and every rights in the copyright to this Work to the University of Malaya ("UM"), who henceforth shall be owner of the copyright in this Work and that any reproduction or use in any form or by any means whatsoever is prohibited without the written consent of UM having been first had and obtained;
(6) I am fully aware that if in the course of making this Work I have infringed any copyright whether intentionally or otherwise, I may be subject to legal action or any other action as may be determined by UM.

Candidate's Signature Date:

Subscribed and solemnly declared before,

Witness's Signature Date:

Name:

Designation:

UNIVERSITI MALAYA

PERAKUAN KEASLIAN PENULISAN

Nama: Tee Wu Yang (No. K.P/Pasport: 950523-01-7303)

No. Matrik: KQK180027

Nama Ijazah: Master of Mechanical Engineering

Tajuk Laporan Penyelidikan Effect of Different Types of Static Mixer Geometry on Quality Microbubble Generation

Bidang Penyelidikan: Fluid Mechanics

Saya dengan sesungguhnya dan sebenarnya mengaku bahawa:

(1) Saya adalah satu-satunya pengarang/penulis Hasil Kerja ini;
(2) Hasil Kerja ini adalah asli;
(3) Apa-apa penggunaan mana-mana hasil kerja yang mengandungi hakcipta telah dilakukan secara urusan yang wajar dan bagi maksud yang dibenarkan dan apa-apa petikan, ekstrak, rujukan atau pengeluaran semula daripada atau kepada mana-mana hasil kerja yang mengandungi hakcipta telah dinyatakan dengan sejelasnya dan secukupnya dan satu pengiktirafan tajuk hasil kerja tersebut dan pengarang/penulisnya telah dilakukan di dalam Hasil Kerja ini;
(4) Saya tidak mempunyai apa-apa pengetahuan sebenar atau patut semunasabahnya tahu bahawa penghasilan Hasil Kerja ini melanggar suatu hakcipta hasil kerja yang lain;
(5) Saya dengan ini menyerahkan kesemua dan tiap-tiap hak yang terkandung di dalam hakcipta Hasil Kerja ini kepada Universiti Malaya ("UM") yang seterusnya mula dari sekarang adalah tuan punya kepada hakcipta di dalam Hasil Kerja ini dan apa-apa pengeluaran semula atau penggunaan dalam apa jua bentuk atau dengan apa juga cara sekalipun adalah dilarang tanpa terlebih dahulu mendapat kebenaran bertulis dari UM;
(6) Saya sedar sepenuhnya sekiranya dalam masa penghasilan Hasil Kerja ini saya telah melanggar suatu hakcipta hasil kerja yang lain sama ada dengan niat atau sebaliknya, saya boleh dikenakan tindakan undang-undang atau apa-apa tindakan lain sebagaimana yang diputuskan oleh UM.

Tandatangan Calon Tarikh:

Diperbuat dan sesungguhnya diakui di hadapan,

Tandatangan Saksi Tarikh:

Nama:

Jawatan:

EFFECT OF DIFFERENT TYPES OF STATIC MIXER GEOMETRY ON QUALITY OF MICROBUBBLE GENERATION

ABSTRACT

This research project is mainly focused on the impact of different types of static mixer on the quality of microbubble generation. The design of the microbubble generation consists of venturi to allow the air intake by using pressure difference and then different static mixer geometry are tested to investigate the effect on bubble rising time and dissolved oxygen (DO). At the first part of study, the work comprises of the relationship of bubble rising time at different pressures and bubble diameter at different pressures. It has proved that higher pressure will induce small bubble diameter and the bubble rising time increases when pressure applied is increasing. Moreover, the factors that influences dissolve oxygen (DO) are studied as well. It is known that longer bubble rising time will have greater DO as the bubble rising time is a representation of bubble diameter. Therefore, it has recorded that the DO surged up by 40% when the diameter of bubble is reduced by 12% in this study. Also, the implementation of different types of static mixer geometry has significant improvement in DO and smaller bubbles are generated. The result is obvious when static glass marbles are used together with static mixer. The DO has been improved by around 10% when 2-phase marbles are applied together with static mixer compared to case with static mixer only. This is a result as greater bubble shredding in turbulence flow is found when multiple static mixers with different geometry are added into the system.

Keywords: Microbubble, Static mixer, Dissolved oxygen (DO), Turbulence flow

EFFECT OF DIFFERENT TYPES OF STATIC MIXER GEOMETRY ON QUALITY OF MICROBUBBLE GENERATION

ABSTRAK

Projek penyelidikan ini tertumpu pada kesan pelbagai jenis pengadun statik pada kualiti penjanaan mikroba. Reka bentuk generasi mikrobubble terdiri daripada venturi untuk membolehkan pengambilan udara dengan menggunakan perbezaan tekanan dan geometri pengadun statik berbeza diuji untuk menyiasat kesan pada masa gelembung yang semakin meningkat dan oksigen terlarut (DO). Ia telah membuktikan bahawa tekanan yang lebih tinggi akan mendorong diameter gelembung kecil dan masa gelembung meningkat apabila tekanan yang digunakan semakin meningkat. Selain itu, faktor-faktor yang mempengaruhi oksigen terlarut (DO) juga dikaji. Adalah diketahui bahawa masa gelembung yang semakin panjang akan mempunyai DO yang lebih besar apabila masa gelembung yang semakin meningkat adalah perwakilan diameter gelembung. Oleh itu, ia telah mencatatkan bahawa DO meningkat sebanyak 40% apabila diameter gelembung dikurangkan sebanyak 12% dalam kajian ini. Juga, pelaksanaan pelbagai jenis geometri pengadun statik mempunyai peningkatan yang ketara dalam DO dan buih yang lebih kecil dihasilkan. Hasilnya adalah jelas apabila guli kaca statik digunakan bersama pengadun statik. DO telah diperbaiki sekitar 10% apabila kelereng 2-fasa digunakan bersama pengadun statik berbanding dengan pengadun statik sahaja. Ini adalah hasil daripada pengecutan gelembung yang lebih besar dalam aliran turbulensi yang ditemui apabila pelbagai pengadun statik dengan geometri yang berbeza ditambah ke dalam sistem.

Keywords: Mikroba, Pengadun static, Oksigen terlarut (DO), Aliran turbulensi

ACKNOWLEDGEMENTS

I would like to take this opportunity to thank to the fine people in UNIVERSITY OF MALAYA for their sincere guidance that I received to support my Master's degree study.

First, I would like to acknowledge my supervisor Associate Prof Ir. Dr. Poo Balan Ganesan who has provided me a lot of guidance and encouragement throughout the project period. In addition to that, he has also assisted me in this research project by sharing his immense knowledge and he has motivated me whenever I felt difficulties. I could not have imagined having a better advisor and mentor for my research project.

Moreover, I would like to thank my parent and brothers who have been supporting me spiritually throughout my life

Finally, I apologize all others unnamed who have assisted me in my Master's degree study.

TABLE OF CONTENTS

LIST OF FIGURES

LIST OF TABLES

LIST OF SYMBOLS AND ABBREVIATIONS

DO	:	Dissolved oxygen
MB	:	Microbubble
MBG	:	Microbubble generation
PIV	:	Particle image velocimetry

CHAPTER 1: INTRODUCTION

1.1 General Introduction

Microbubbles are defined as bubbles which have bubbles diameter size between 50µm to 200µm. Microbubbles have several characteristics, such as larger interfacial area, higher mass transfer rate and low rising velocity (Tsuge, 2010). Due to these characteristics, microbubbles are implemented in various fields and the most common applications are aerations, water treatment, drag reduction of ships, medical use, etc.

There are few methods to generate microbubbles, among them are spiral liquid flow, ejector, electro flotation, venturi and pressurized-dissolution methods (Terasaka et al., 2012). Venturi method is one of the famous microbubbles generation (MBG) method used by others due to its low cost and effective characteristics for MBG. Venturi-type MBG operates in such way that it allows a liquid stream which contains macro size bubbles to flow from the inlet of a venturi tube. When it flows through the constricted region, air will be sucked in as a result of pressure change, thus the macro size bubbles will be reduced to microbubbles by cavitation. However, the disadvantage of venturi type MBG is the coalescence of small bubbles which result in big bubble generation at the outlet of the venturi. Nevertheless, the recent research showed that by adding 50 ppm 3-pentanol, 100 micro meter of microbubbles are mainly produced (Fujiwara, 2006).

Figure 1.1: Microbubble generation in a venturi tube (Tsuge, 2016).

Microbubbles are difficult to capture in image form as the size of microbubble is very tiny, thus scientists have come out with some measurement methods to quantify and qualify microbubble as it is essentially important to understand the behavior of microbubble for the purpose of application. Up to now, several studies have demonstrated the measuring methods of size of microbubble, namely visualization method, laser diffraction or scattering method and also particle image velocimetry (PIV).

1.2 Importance of Study

The findings of this study, by considering the tremendous benefits of microbubble application, play a vital role in science and technology today. In addition, aquaculture business in Malaysia has been deteriorating due to the poor technique and less research-focused on the possibility and potential of new technology or method to cope with the increasing demand of aqua-farming. Hence, a new approach will be uncovered in this study to examine the potential of this microbubble generator in boosting the dissolved oxygen (DO) in aquafarm because dissolved oxygen is the function of the yielding rate of aquafarming.

1.3 Problem Statement

Fresh water fish is one of the most promising sources of protein because it is relatively faster in both breeding and growing compared to other protein source such as cattle and poultry. Nevertheless, it was found that the production of freshwater fish in Malaysia has not even close to be the main supplier of increasing domain from international market. The main objective for that is lacking technology penetration in this prospective sector. Therefore, microbubble technology is introduced to increase the number freshwater fishes.

According to Thean et al (2016), shrimp aquaculture is quite intensive in Malaysia, but the productivity of shrimp is relatively lower compared to neighboring countries including Vietnam, Thailand and Indonesia. Dissolved oxygen is a significant factor in aquafarming as the water conditions and oxygen level inside the water is a decisive indicator of whether the production level of aquaculture in Malaysia is growing or reducing.

Microbubble aeration is one of the techniques that has been adopted to boost the production rate of aquaculture in Malaysia. However, due to its high initiation cost and skill-required characteristics, many of the aqua-farmers have retreated to invest in such technology. Also, difficulties in rising production cost, land acquisition and threat of diseases are factors that impede the development of aquaculture in Malaysia. The purpose of this project is to adopt a new microbubble generation or aeration technologies as a benchmark for aquafarming to improve the total aquaculture production in Malaysia as research showed that the total aquaculture production in Malaysia has experienced a significant a substantially drop since 2010.

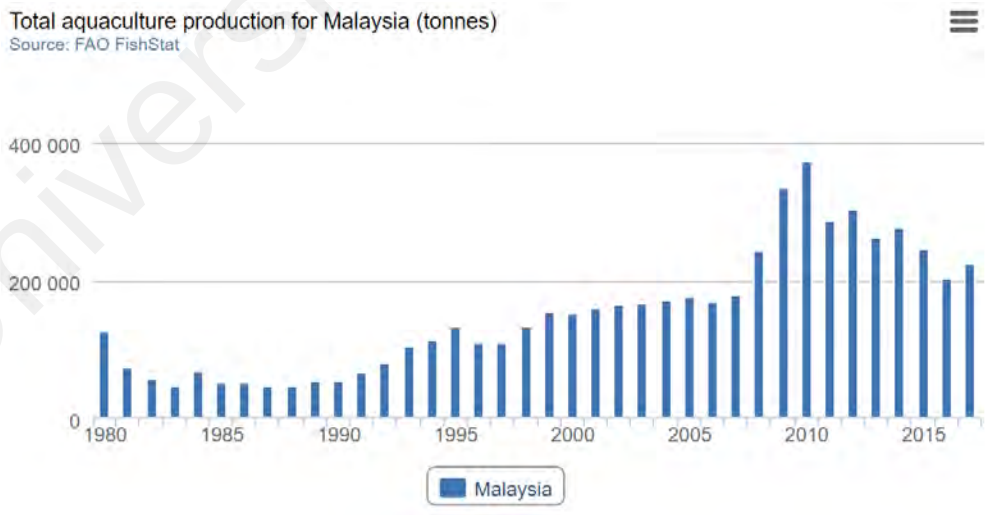

Figure 1.2: Total aquaculture production for Malaysia from 1980 to 2017. (FAO, n.d.)

1.4 Aim and Objectives

The aim of this study is to examine the effect of different types of static mixer geometry on quality of microbubble generation, with the objectives below:

1. To develop a bench scale microbubble test experiment setup
2. To investigate the dissolved oxygen (DO) and diameter of microbubble generated from different dispersing elements.

1.5 Scope and Limitation of the Study

This study will focus on developing a bench scale microbubble generator using venturi, static mixer and static marbles mixer. Different dispersing elements will be implemented to produce different size of microbubbles. In addition, the quality of the microbubble will be studied to understand the effect of each dispersing element on the production of microbubble. Other than that, the water supply that used to generate the microbubble will be the tap water supply for UM lab. Visualization method is the method used to estimate the size of the microbubbles, whether the quality of microbubble is being affected when tested with different tools use such as static mixer, marbles and 2-phase marbles. The data collection will be working on microbubble condition at different pressure as well. The limitations of this study are the visualization measurement method, conditions of dissolved oxygen of the tap water and lastly the preparation of the microbubble solution sample.

1.6 Contribution of the Study

The finding on this study will provide an insight on the improvement of water quality especially for aquaculture such as fish and shrimp. The importance of microbubble will not only benefit fish and shrimp, it will also have impact on the water treatment industry whereby low-cost water treatment can be implemented with high efficiency. Moreover, the technique that used to generate microbubble in this research project will help to understand better about the performance of microbubble under different setup. For instance, the effect of geometry on the quality of microbubble will help to uncover some of the relationships between the quality of microbubble generation and different parameters. Thus, the feasibility of dispersing element can be verified with the data collected.

CHAPTER 2: LITERATURE REVIEW

In this chapter, reviews are mainly focused on the properties and characteristic of microbubble, microbubble generation methods, microbubble measurement methods and fluid flow of different geometry.

2.1 Microbubbles

Microbubbles are generally referring to bubbles that are of micrometer order, their size is less than 100 micrometers for fluid physics and for bioactivity the size is 10-40 micrometers. It has a very slow rising velocity, takes for example to rise 20cm in 1 hour the microbubble size needed to be less than 10 micrometres. On the other hand, the pressure inside microbubble is of very high pressure and according to Tsuge (2014), inner pressure of bubbles with diameter of 1μm and 100nm are 3.87atm and 29.7atm respectively. Besides, the gas dissolution rate increases as the bubble size decreases. In other words, bubbles will experience an inner pressure increment as the size of bubble decreases. Simultaneously, the driving force of dissolution is generated as the dissolved gas component undergoes increment in partial pressure which in turns increase the dissolution rate of gas effectively.

Apart from that, microbubble is proven to have the capability to reduce friction drag which it has been experimentally tested by injecting microbubble from the bottom of big ship. There are studies showed that microbubble possesses bioactivity effect, Ohnari (2007) had verified that the blood flow rate of oyster in Hiroshima had improved noticeably, and again an increasing trend of the blood flow rate of scallop and pearls in Hokkaido and Mie prefecture respectively which ascertained the effect of bioactivity by microbubble. In the following topics, the characteristics and properties of microbubbles will be further discussed and application of microbubble as well.

2.1.1 Size

The size of bubbles can be categorized into 3 classes, which are macrobubble, microbubble and nanobubble. Macrobubbles are bubbles that can be observed in daily life as it has a diameter greater than 5mm. In general, macrobubbles have higher rising velocity than others, which causes it to rise rapidly to the surface of water and burst at the interface of air-water.

Microbubbles (MBs) are small, gas-filled bubbles with bubble size between 50μm to 200μm, which is close to human hair (70μm). MBs usually shrink in water and disappear completely in the water by dissolution. According to Takahashi, Chiba and Li (2007), a white cloud dispersion as a result of MBs will be formed in the water and last for few minutes depending on the MBs size.

Besides, nanobubbles are bubbles that have extremely high internal gas pressures. The diameter size of nanobubbles are smaller than 20nm and the pressure found inside a 20nm diameter nanobubble is 14.5MPa. As a result, it shows a rapid dissolution of nanobubble in ambient liquid. An equation was developed by Li Juan et al. (2008) to estimate the lifetime of nanobubbles:

$$\tau = \frac{H d_0^3 \rho_g}{48 D \gamma \left(1 - \frac{\rho g}{\rho_1}\right)^4} \quad (1)$$

Hence, the lifetime of nanobubble increases as the density of gas presented in nanobubble increases.

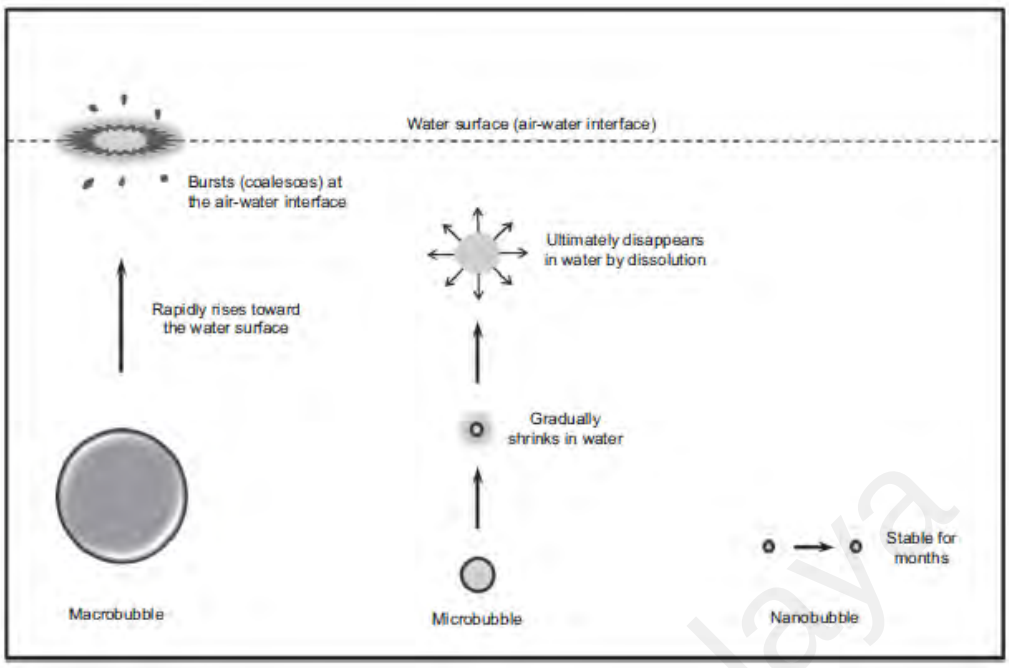

Figure 2.1: Difference between macrobubble, microbubble and nanobubble in terms of their behavior in water (Takahashi et al., 2007).

2.1.2 Microbubbles Formation

The most general way for the formation of microbubble works by blowing the gas under pressure via orifices in a component named aerator, where the bubbles will be further divided into smaller bubbles at the exit of the aerator. Despite of these very small pores mechanism is used, the instability of bubbles due to surface tension will cause the bubbles to coalescence and grow bigger. Hence, researchers had investigated the possibility to form the microbubble which is to break the bubble by shear stresses in turbulent flows. One of the examples for formation of microbubbles through turbulent flow is depicted in figure 2.2. There are a few microbubble formation methods that are being used, each with various disadvantages and advantages and they will be discussed in the following topic in this chapter.

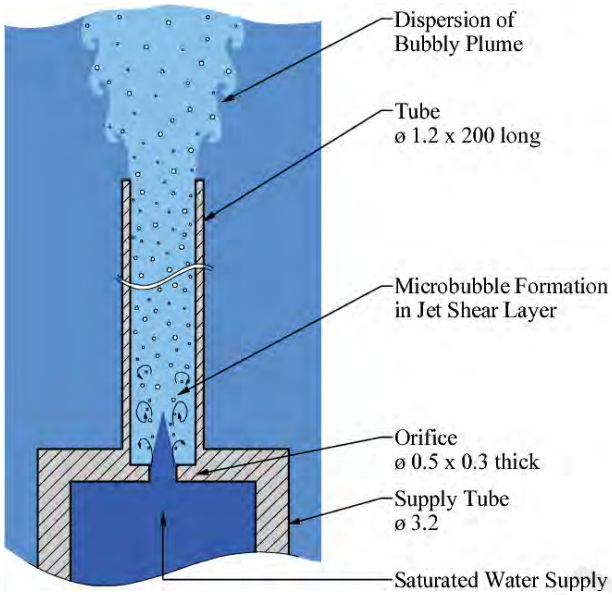

Figure 2.2: Formation of microbubble through turbulent flow (Brandner et.al., 2010)

2.1.3 Chemical and Physical Properties of Microbubble

In general, there is a misconception regarding microbubbles, which they are claimed to be similar with large bubbles in terms of chemical and physical properties, the only difference is their size. Many researchers had considered the diameter of microbubble just a convenient and simple number, where d= 1mm. However, studies have uncovered that microbubbles are qualitatively different from large bubble, either their chemical and physical properties.

First, microbubbles have very high internal pressure that create almost impossible deviation from sphericity. While the large bubbles have restriction in their sphericity that large bubbles cannot achieve a perfect spherical shape. Owing to the hydrostatic pressure difference between the bubble bottom and top, the geometry of large bubbles undergo deformation even if they are at stationary state.

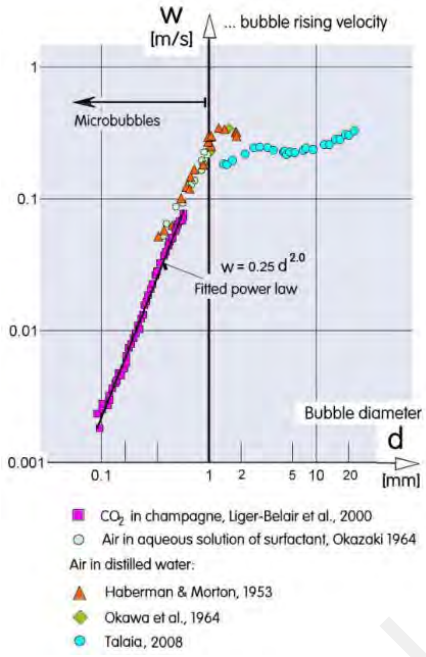

Figure 2.3: Rising velocities of large bubbles and microbubbles in liquid (Zimmerman et al., 2008).

Next, microbubbles and large bubbles share the same behavior as they ascent in liquid towards the surface above. However, large bubbles will have the tendency to deform as a result of hydrodynamic force. Perhaps rather surprisingly, the trend of the ascent velocity dependence on the diameter of bubble, d varied for both cases. Detailed studies revealed that the rising velocity of microbubbles are proportional to their diameter. While the ascent velocity of larger bubbles differs in a complex way, which the velocity shows insignificant changes as the bubble diameter increases, as shown in Figure 2.3.

Other than that, the heat transfer of large bubbles and microbubbles vary in propagation process. From Figure 2.4, it indicates the heat propagation occurs in both large bubbles and microbubbles, in which a boundary layer is formed when heat propagation takes place. There is a likelihood that the thickness of the boundary layer grows as heat propagates towards the large bubbles but not effectively transfer throughout the internal space. For microbubbles, heat is being transferred simultaneously throughout the full internal space of microbubbles because the size of microbubbles is very tiny that causes all the gas being heated compared to large bubbles that presents with heater gas layer only as a result of effective heated region. This is mainly because the effective distance of diffusive transport in the gas is influenced by the diameter of bubbles. In order to have all the gas heated thoroughly in the internal space, the diameter of bubbles must be smaller than the distance of diffusive transport, otherwise only heater gas layer will be formed.

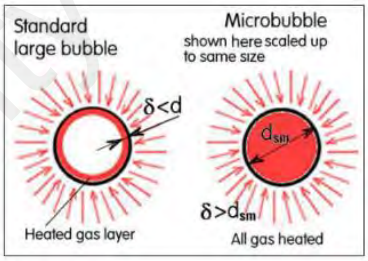

Figure 2.4: Heat propagation of large bubble and microbubble (Sadatomi et al., 2012).

Microbubbles have large interfacial area which contributes to the gas dissolution fraction as:

$$\frac{A}{V} = \frac{6}{d} \tag{2}$$

When the interfacial area increases or the diameter of bubble decreases, the gas dissolution fraction increases. Hence, the dissolution rate of dissolved oxygen (DO) for microbubble is greater than that of large bubbles. Furthermore, the mass transfer rate N can be calculated using the inner pressure of bubble and the liquid phase mass transfer coefficient k_L. When the surface area of a large bubble with diameter of 1mm is defined as 1, the surface area will vastly increase as it segregates into smaller bubble or microbubble. Take for example, 6×10^4 times of surface area increment is gained when 1mm of bubble segregates into $1\mu m$. According to this equation:

$$N = k_L A(p - p^*)/H \tag{3}$$

microbubble with greater surface area will yield a better mass transfer rate, if mass transfer rate of 1mm bubble, denote N to be 1, the mass transfer rate of $1\mu m$ will become 10^8 as the rising velocity of microbubble decreases. So, the dissolution rate can be increased rapidly by using microbubbles in oxygen-water system.

$$k_L = \frac{D_L}{d}\left[1 + \left(1 + \frac{dU}{D_L}\right)^{1/3}\right] \tag{4}$$

Besides, Himuro (2007) stated that when microbubbles are generated in city water under temperature of $25°C$, viscosity of the liquid and the surface tension decrease substantially and observation with improvement on electrical conductivity as well. This is because the hydrogen bond among the water molecules undergo changes in cluster by cleavage of the bond and the city water has experienced ionisation of chemicals. Ahmadi et al (2014) claimed that the magnitude of zeta potential, ζ of bubble can be related to the size of microbubble. As the size of bubbles changed from 500nm to 10μm, the zeta potential, ζ decreased from 21mV to 17mV. The zeta potential further reduced after the generation of microbubble and 15mV was recorded after 10 minutes of Nano microbubble generation. It was due to the coalescence of bubbles that caused by the reduction of zeta potential over time.

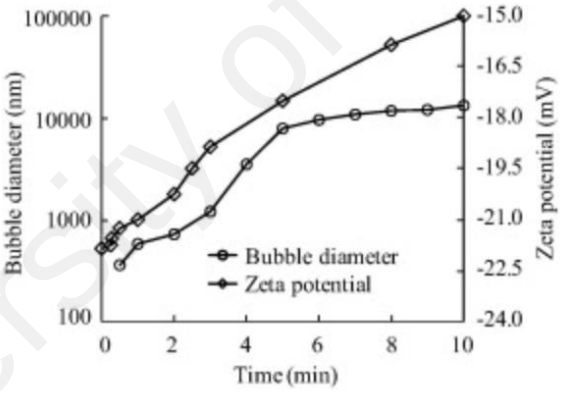

Figure 2.5: Relationship of zeta potential and bubble diameter over time (Ahmadi et al., 2019).

Dissolved oxygen reflects the quality of water as either low or high oxygen level can harm the aquatic life such as bacteria, fish, plants and invertebrates. These organisms consumed oxygen for respiration just like human being and organisms on land. Phytoplankton and plant life need dissolved oxygen to carry out respiration when there is no enough light for photosynthesis. Similarly, crustaceans and fishes acquire dissolved oxygen through their gills for respiration as well.

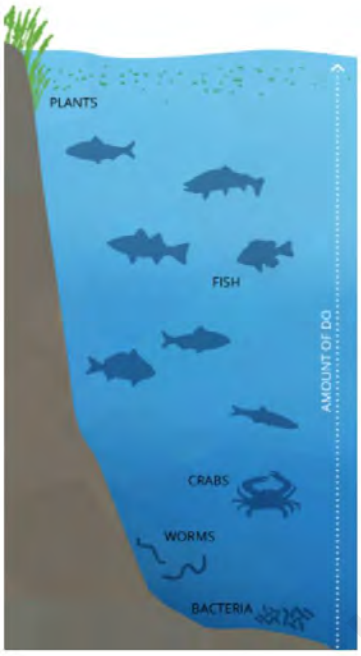

Figure 2.6 Dissolved oxygen (DO) as a main source of respiration for many forms of aquatic life (FONDRIEST, n.d.)

According FONDRIEST (n.d.), a minimal of 1-6 mg/L of dissolved oxygen (DO) is needed for organisms including crabs, worms, bottom feeders and worms while 4-15 mg/L of dissolved oxygen (DO) is required for shallow water fish to sustain in water. Therefore, it is essentially important to provide adequate DO to aquatic life to ensure the sustainability of ecosystem so that ecological balance can be attained.

2.2 Application of Microbubbles

Microbubbles are widely implemented by various industries, including medical, logistic, aquafarming, water treatment, etc. Take for example, there have been cases where microbubble is used to improve the drag force in logistic application, to provides information of the blood for the ease of diagnosis, to increases the efficiency of chemical treatment of water and so on. The maturity of microbubbles technology is yet to be discovered as more and more researches have further encountered the potential of microbubbles which could play an important in bringing significant impact to our daily life.

2.2.1 Reduction of Drag Force in Logistics Application

Nowadays the logistics industry is focusing on improving fuel efficiency as fuel cost is the function of a logistic company's revenue and government also advocates to reduce the emission of greenhouse gas (GHG) as part of the plan to promote an eco-friendly environment. Hence, researchers had invented a way to reduce the drag force of ships which is covering the surface of a ship that moves inside water with minutes air bubbles through air bubbles injection onto the surface of the ship.

McCormick et al. (1973) are the first batch of researchers that involved in the studies of air bubble drag reduction. During the experiment, hydrogen bubbles were produced by electrolysis on copper wires that wrapped on the aft part of a body with axi-symmetric and maximum diameter 0.27m and 10-20 % drag reduction was obtained. They had stated that the electric current is the function of the magnitude of drag reduction and higher drag reduction was achieved by increasing the electric current. However, the drag reduction reduced when the higher speed was encountered.

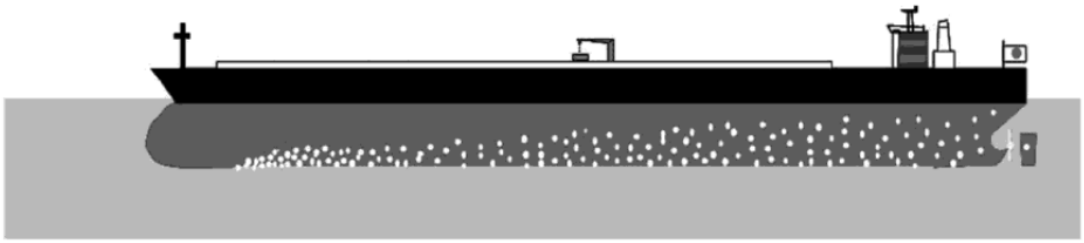

Figure 2.7: Application of microbubbles to reduce drag of ship (Tsuge, 2014).

According to Tsuge (2014), the largest ship is with width that more than 60m and length longer than 400m and shapes of the hull are boxy to cater for high loading efficiency. The cruising speeds of these kinds of ships are relatively slow, normally around 7.2 m/s or 14 knots. Owing to this factor, the drag contributed by wave component is very minor that making the drag of friction to be dominant, reaching 80% of total drag. As shown in Figure 2.6, air bubbles are injected at the forward part of the ship and as a result of buoyancy the air bubbles stick to the hull surface as they go downstream. Moreover, wider area is covered and significant reduction on skin friction is attained.

The equivalent air layer thickness, t_a (assuming flows along solid wall with uniform speed) is defined as

$$t_a = \frac{Q_a}{U_\infty B_a} \tag{5}$$

where U_∞ denotes the advancing speed of ship, B_a denotes width of injection area and Q_a denotes the air injection volume per unit time. The skin friction ratio C_f/C_{fo} where C_f is the skin friction with injection of air bubbles and C_{fo} is skin friction without injection of air bubbles. The skin friction reduction is obtained when Q_a increase and the maximum reduction that can be achieved is 80%. Though skin friction effect is not speed dependence, but the data collected shows that the effect of skin friction shows difference when speed started to increase. The skin friction reduction is effective when the thickness of air layer (injected air bubbles) increases and the maximum reduction effect occurs when the thickness of t_a reaches 7mm.

2.2.2 Imaging and therapeutic

Normally, people will think about putting bubbles into the human body, which is not a very good idea. One of the examples is these bubbles are associated with causing the bends that can be encountered in scuba divers. Bubbles that are extremely small such as microbubbles can pass safely through the human blood vessels without causing a blockage. This is because the image of ultrasonic scan that people see on the screen is all about the density of the tissue in human body (Stride and Coussios, 2010). Moreover, if the density can be changed, one area of that will become much clearer compared with another. By putting gas into human bloodstream, even with very tiny amounts it can create a big density change which gives a very strong ultrasound echo. Hence, clinicians will be able to trace where blood is flowing much more easily and enhance detection if there are any problems.

2.2.3 Drug delivery

Microbubbles are applied in drug delivery as well whereby they are used as vehicles to transport small amounts of drag. The bubbles are coated with little shell of polymer that the drug is dissolved in. Next, the bubbles are traced through the body and they can be observed under ultrasound imaging so that the direction of microbubbles can be identified. Once they reach the site of where clinicians want to target, for example, the tumour, the ultrasound power is turned up to break the bubbles and release the drug (Stride, 2009). As a result, the released drug can be localized and any harmful side effects can be minimised such as cancer chemotherapy.

2.2.4 Water treatment

According to Argawal, Ng & Liu (2011), MBs possess the ability to create highly reactive free radicals so MBs are potential in water treatment. Research had shown that MBs are used for water detoxification and it also help the anaerobic and aerobic microorganism activities in submerged membrane bioreactor. Owing to the ability to catalyze chemical reactions, MBs have found to be effective in detoxification, which increases the chemical treatment efficiency of water.

The main reason to implement pretreatment of water is to increase the treated water quality and decrease the running costs by reducing the loads in terms of chemical, biological and physical. There are few water treatment examples with MBs technology, which are disinfection of water, defouling and cleaning of solid surfaces

2.2.5 Disinfection of Water

During the generation of MBs, it is often associated with turbulence and highly reactive free radicals, which are beneficial to the water disinfection. Under various conditions, ozone MBs was observed to have higher disinfection kinetics of E, coli, which led to a smaller reactor size and smaller ozone dose when comparing to the ozone disinfection using conventional method for identical disinfection efficiency of a 2-log inactivation (Sumikura et al., 2007). Moreover, the shock wave and OH radical are the reasons for inactivation of coliform but the contribution to this effect still remain unknown. The hydrodynamic cavitation that generates MBs is useful to increase the deactivation efficiency of E coli in water disinfection.

2.2.6 Defouling and Cleaning of Solid Surfaces

MBs have been implemented for the removal and prevention of adsorption of proteins on to solid surfaces. According to Agarwal, Ng and Liu (2011), MBs can inhibit the proteins from being adsorbed onto various surfaces which eventually prevents the surfaces from fouling. Take for example, bovine serum albumin which adsorbed on mica surface can be inihibited by MBs, MBs also help to separate the organic contaminants from gold surfaces and pyrolytic graphite. Other than that, it was also observed that similar defouling effect of MBs on stainless steel surface.

This is because the bubble size is capable to influence the fouling of membrane in hollow fiber membranes and tubular as well (Tian et al., 2010**)**. Next, it was found that the intermittent bubbling is less effective than continuous air bubbling in fouling control due to the scrubbing of air bubbles on the membrane surface during the filtration process, thus reducing the layer of fouling on membrane and concentration polarization. Furthermore, smaller size of air bubbles is also effective in reducing fouling.

2.2.7 Aquafarming

According to the research carried out by Ebina, Shi and Hirao (2013). The effects of nanobubbles on the growth of fishes, sweetfish were observed and examined for 3 weeks. Some of the parameters were set such as the nanobubble aerator was always operating in a condition where 67 litres of air-nanobubbles water per minute were circulated and fish baits that equal to 13% of the total weight of fishes were provided per day in each group. In addition, the data collected shows that the oxygen concentration which was 7.7 mg/L initially in distilled water shoot up to 31.7 mg/L immediately after the nanobubble system was run for 30 min with 100 liters of water.

It was reported that the weight of the sweetfish increased from 3.0 kg to 10.2 kg in the case where air-nanobubble system is used in normal water and the total weight of sweetfish in normal water changed from 3.0 kg to 6.4kg in normal water. So, the nanobubble system was proven to have the ability of increasing the growth rate of fishes by around 300% compared to the 100% growth of fishes in normal water.

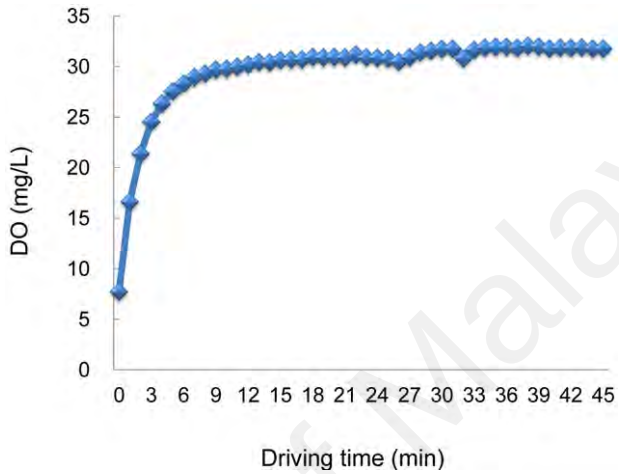

Figure 2.8: Dissolved oxygen in nanobubble system over time (Ebina, Shi and Hirao, 2013).

2.3 Microbubble Generation

Microbubble has been a highly discussed topic since few decades ago due to its various functions in different applications. Several methods had been discovered by researchers and scientists including venturi, fluidic oscillation, dissolved air floatation, induced air floatation, electro-floatation, swirl flow method, static mixer and porous method. The operating principle of these methods will be discussed in the following chapter and the advantages and disadvantages will be studies as well.

2.3.1 Methods

2.3.1.1 Venturi Type

The working principle of venturi comes from Bernoulli's principle, which it states that the total energy available in a fluid that flows along a path (enclosed) is identical at any two points in that path. When a fluid is forced to flow through a constriction in a venturi tube, the velocity of fluid increases in the throat, which induces a pressure drop. Then, that substantial pressure drop leads to a generation of suction force and air from the atmosphere is being sucked into the venturi tube without external force. This is where the mixing of air and water occurs when water is pumped by a centrifugal pump. Moreover, MBs are generated with proper combination of air and liquid flow rates and pressure (Henderson, n.d.).

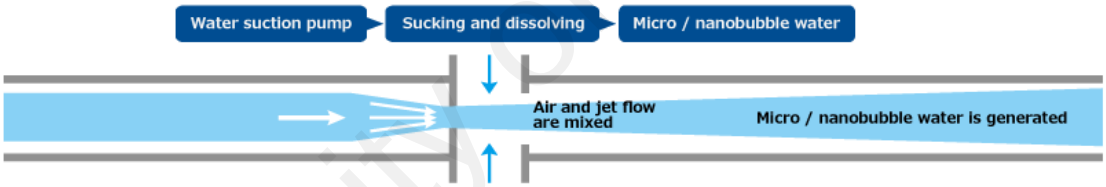

Figure 2.9: Microbubbles generation using venturi tube (Henderson, n.d.).

2.3.1.2 Fluidic Oscillation

It is now well established from a variety of studies that microbubbles can be generated by issuing pulsating to the inlet gas flow through a fluid oscillator. Fluidic oscillator consists of two components, which are fluid flow field with amplification properties and a negative feedback. The first component possesses a sensitive spot due to its cavities for the flow that have been shaped, as shown in Figure 2.9. Besides, amplification of the system will trigger a relatively weak input flow that leads to a large change of the whole flow field. What the negative feedback does is it creates oscillation by destabilizing the

conditions in which part of the output fluid flow will be returned to the feedback loop (Tesar, 2017).

The configuration of the fluidic oscillator is shown in Figure 2.9, where it comprises of few terminals, namely S (supply), Y (Output), X (Control) and V (Vent). As shown in figure 2.9, supply terminal S acts as a medium where it brings fluid flow into the amplified device. Then, it will amplify the weak signals and then disperse through output terminal Y. Meanwhile, part of the output flow that has been amplified will be returned into control inlet X. In order to have the feedback mechanism works effectively in a fluidic oscillator, there are two features needed. First, the main flow channel S must be designed in converging manner so that the increasing fluid flow will decrease as it exits Y. Other than that, it has also been suggested that phase delay must be included in the loop as fluid flow takes time to get from Y to X.

The fluid oscillator works by introducing air flow to enter via the supply terminal S and a jet is formed by the supply nozzle, as shown in figure 2.10 as the curved blue line. As a result of Coanda effect, the attachment wall p will be attached by the jet and will be led into the output terminal Y where this terminal is shaped as a diffuser (Tesar, 2017). In other words, the terminal Y is in diverged form so as to ensure the fluid flow can perform in a gradually increase manner. So, energy conversion happens at the nozzle area where input pressure energy is converted to kinetic energy. The airflow will be slowed down in the diffuser as the pressure increases. Thus, the pressure at the interaction region near the wall p is found to have a minimum pressure which is lower than the pressure presented in Y. Hence, the air flow will be driven via the feedback loop channel as a result of pressure difference.

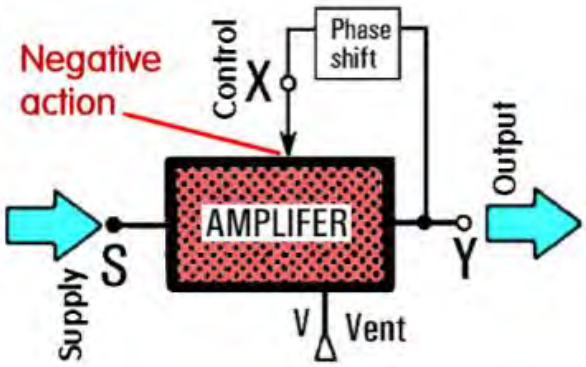

Figure 2.10: Basic configuration principle of fluidic oscillator (Tesar, 2017).

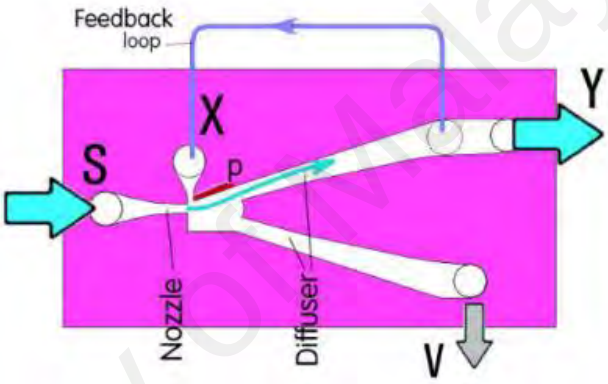

Figure 2.11: Design of a simple fluidic oscillator (Tesar, 2017).

2.3.1.3 Dissolved Air Flotation (DAF)

Dissolved air flotation (DAF) is one of the MBs generation method that has been widely used in the treatment of potable water. For this method, air is pressurized into fluid at high pressure, then the pressurized fluid is then released and decompressed through injection of nozzles at atmospheric pressure. Bubbles will be formed, adhere to the surface of solid particles and rise to the surface of the liquid when the air is transferred out of solution and pressure will be reduced. So, the solid particles will float to the water surface and it can be removed by a skimming device. The MBs that generated using DAF normally have a diameter range of 10-120μm, with a mean diameter of 40 μm (Li and Tsuge, 2006 DAF 2nd).

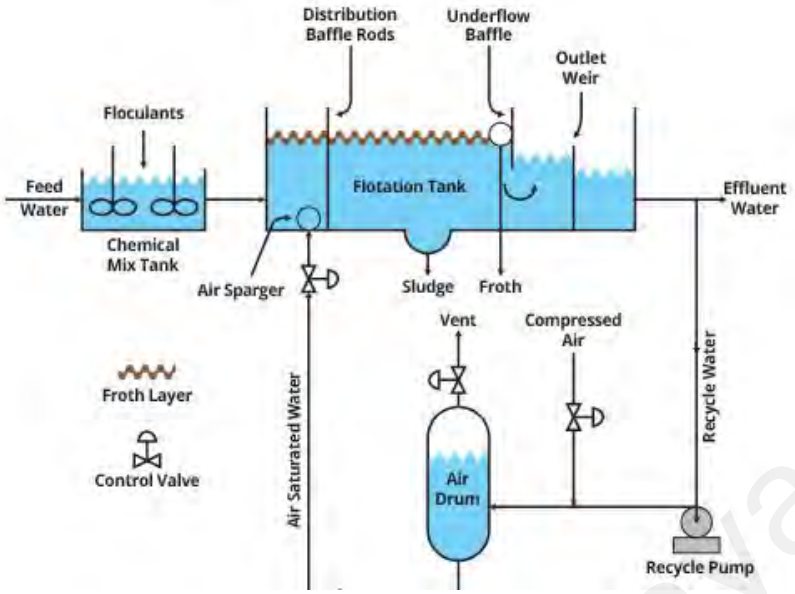

Figure 2.12: A typical Dissolved Air Flotation (DAF) unit (Aquacache, n.d.).

2.3.1.4 Induced Air Floatation

Apart from dissolved air floatation, another floatation method is induced air floatation. The operating principle of induced air floatation is by saturating the water through permitting air to go into the pump's suction side or carry out the water-air saturating process inside aeration tank. As shown in Figure 2.12, the recycle water is fed in to the cylindrical tank with flow rate, F_W and a rotating flow is generated along the cylindrical inner wall. This will help to induce the air from bottom of the cylindrical tank as a result of pressure difference and the air bubbles are shattered and cut by the water flow and eventually several minutes bubble is being discharged from the upper part of the generator (Tsuge, Li & Hirofumi, 2004).

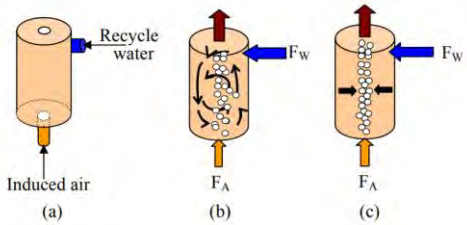

Figure 2.13: Induced air floatation to create microbubble (Tsuge, Li & Hirofumi, 2004).

2.3.1.5 Electro-floatation

Recently, a new method has been developed to generate fine bubbles, which is electro-floatation. This technique able to generate microbubbles to take away the low-density particles from water via electrolysis of water. It has a high removal efficiency and very easy to operate compared to others thus being considered effective. Many water treatment industries have started to implement electro-floatation to replace conventional dissolved air floatation due to the reason that the bubbles size generated by electro-floatation is much smaller and the charge of the bubbles can be manipulated. Han, Kim and Ahn (2006) had stated that the charge on the bubbles can be induced with positive charge instead of negative charge under normal conditions which will influence the removal efficiency of bubbles. The setup of electro-floatation is demonstrated in Figure 2.13.

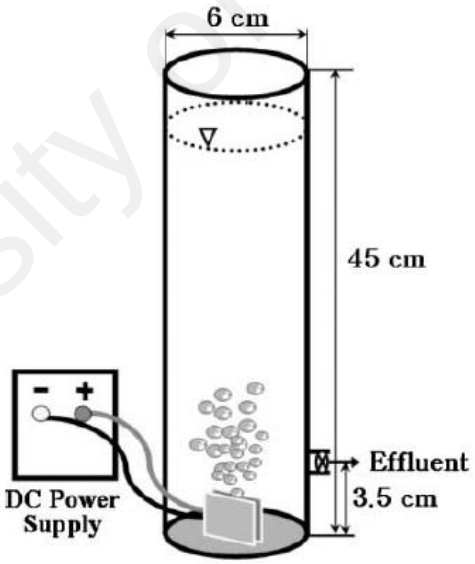

Figure 2.14: Demonstration of electro-floatation to generate microbubbles (Han, Kim & Ahn, 2006).

2.3.1.6 Swirl Flow Method

Swirl flow method is another type of microbubble generation technique which encompasses the concept of venturi together with nozzle to induce a very strong turbulent flow. The details drawing of a general swirl flow microbubble generator is shown in Figure 2.14.

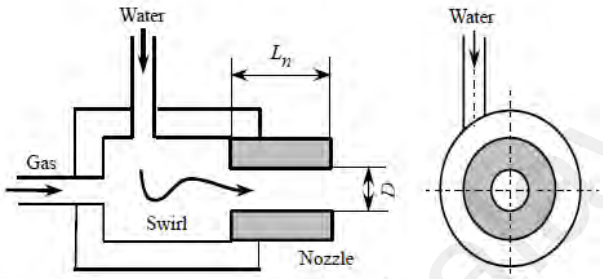

Figure 2.15: Swirl flow microbubble generator (TABEI et al., 2007).

It comprises of swirl chamber, decompressor, cylindrical nozzle and measuring devices such as pressure gauge, flow meter and dissolved oxygen (DO) meter. First, the pressurized water is being sucked in by the pump and circulated into the decompressor. Therefore, self-suction of the air occurs as a result of formation of negative pressure of swirling flow and eventually leads formation of air bubbles occurs and the air bubbles will be dispersed into water (TABEI et al, 2007). So, air bubbles will undergo breakup into minutes bubbles due to turbulent flow. Next, the air-water mixture will spread out uniformly through the outlet or nozzle, as shown in Figure 2.15.

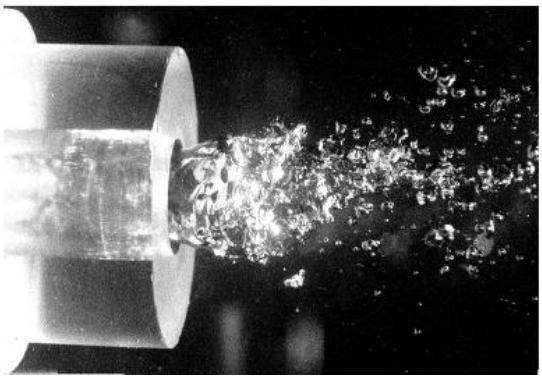

Figure 2.16: Water flow condition at the nozzle of swirl flow microbubble generator (TABEI et al, 2007).

2.3.1.7 Static mixer

Static mixer, which also known as motionless mixer has been widely used as inline mixer for the purpose of cooling/heating and reaction of low and high viscosity liquids, gases, slurries and the contacting of solids, gases and liquids at multi-phase. Besides, static mixer is also used as inline mixer to boost the process of mixing and dispersing (Statiflo, n.d.).

In addition, materials with equal or different volumetric flow rates and viscosities able to mix well with the aid of static mixer. The fluid that pass through the mixer will be stirred by elements and thus sequentially mixed (Noritake, n.d.). The most common static mixer is made up of parts that consist of left and right element whereby a rectangular plate is twisted 180 degrees, generating a left element and a right element, based on the direction of the twist. The length of each element is about one and a half times of the diameter. The configuration of left element and right element is shown as:

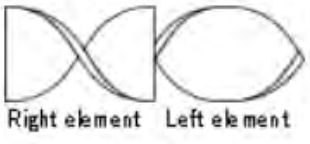

Figure 2.17: Internal configuration of static mixer (Noritake, n.d.).

Moreover, static mixers are useful for homogenizing fluids which requires no moving parts, especially in continuous process. Take for example, blowers or pumps that are applied in continuous process operate to transfer the components to be mixed at favorite volumetric flow rates and to also provide the required pressure energy for mixing. The sizes of static mixer normally range from small units (laboratory size) that fits into 3/16" diameter tubing, process piping that varies from one forth inch Sch.40 to over 120" diameter and rectangular or square conduit such as 46ft by 13ft for flue gas treatment in power plant.

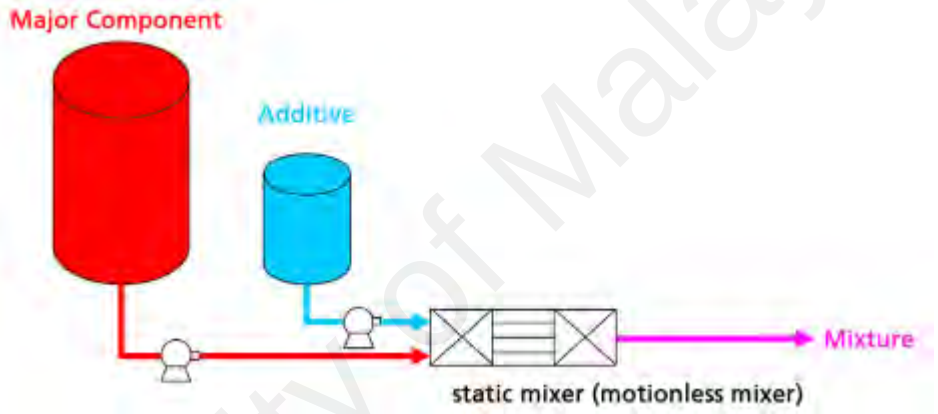

Figure 2.18: Static mixer that used in continuous process to create mixing homogeneously with no moving parts in short length (Stamixco, n.d.).

There are few types of static mixers, one of them is X-grid static mixer, where individual mixing elements that arranged in series order by stacking with each other. Each of the mixing elements is oriented 90 degrees corresponding to the adjacent mixing element so that both the vertical and horizontal directions will have homogeneous mixing (Stamixco, n.d.). In order to ensure the stream at the outlet of static mixer is homogeneous in respect to velocity, concentration and temperature which are equalized throughout the cross-section of pipe entirely, the elements inside recombine and divide the feed materials.

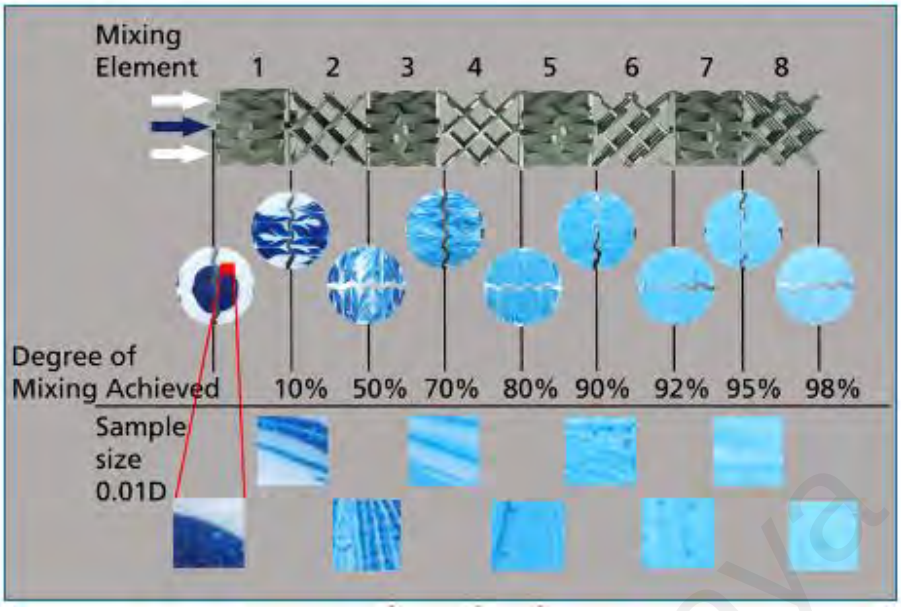

Figure 2.19: X-grid Static mixer that stacked in series to achieve homogeneous mixing (Stamixco, n.d.).

Next, there is another static mixer known as helical static mixer where it has a series of helix shape elements that attached to each other. The performance of helical static mixer is dramatically lower than that of X-grid static mixer, however, the helical static mixer is still used extensively mainly due to its open non-fouling design and lower pressure drop compared to X-grid static mixer.

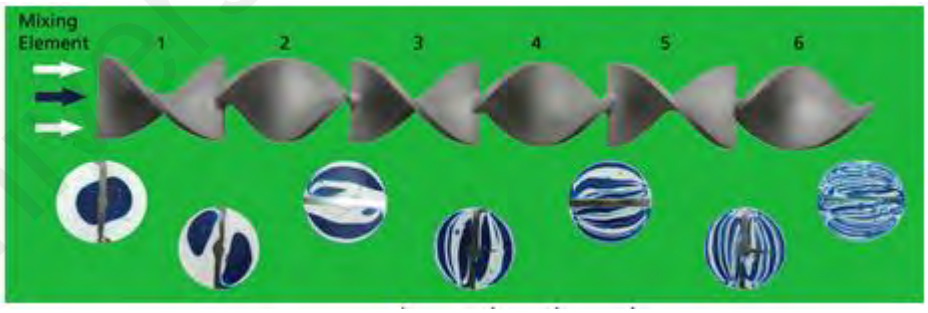

Figure 2.20: Helical static mixer (Stamixco, n.d.).

Generally, the static mixer goes through 3 different processes simultaneously to mix efficiently, which are division, conversion and inversion. Division process is a process where the liquid is split in half each time it passes through an element inside the static mixer and the number of separations rely on the number of elements. For example, a static mixer that has 4 elements will encounter 2n (n equals to number of elements) times of separations which is 8 times. When the fluid passes through the first element, it is split into 2 flows, then the next element further divides the flows into 4 flows, continuous until 8 divisions are achieved at the fourth elements.

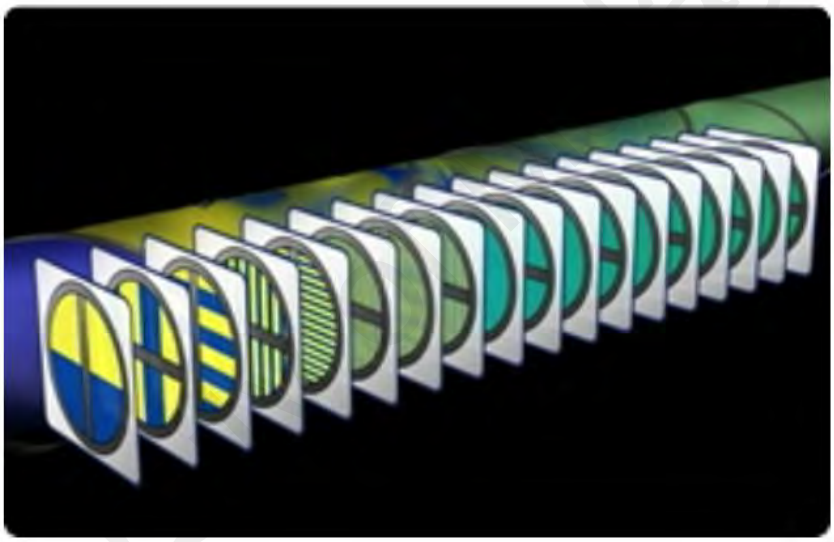

Figure 2.21: Division process in static mixer (Noritake, n.d.).

Then, when the elements of inner spiral walls are filled with fluids that glided along them, the movement will cause the fluids to pass through the center part of the cylinder to the walls. Also, the fluid will move from the walls to the center part and the mixed fluids will be sorted, this process is known as conversion. In the case of helical static mixer, when the direction of the flow changes along the streamline surface of the twisted shaped element the flow is rotated in the direction of the axis. Under this force, the fluid in the center section of the pipe is moved to the peripheral section and the fluid in the peripheral part of the pipe is moved to the center section as it is pushed.

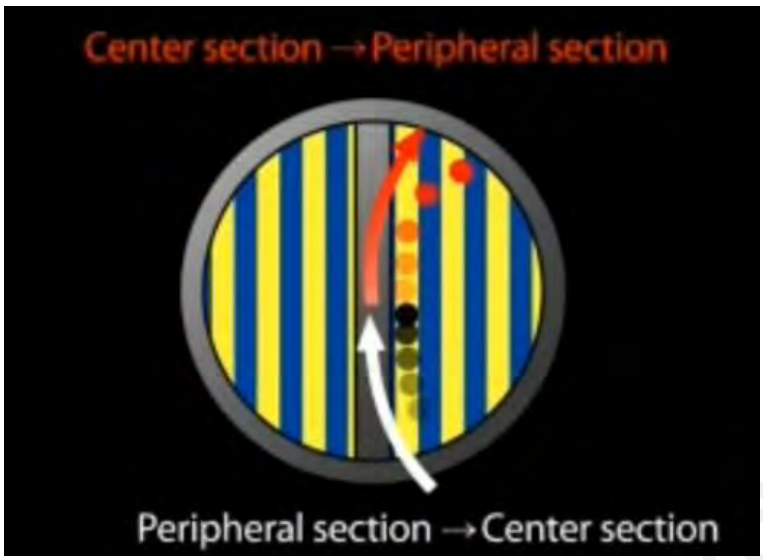

Figure 2.22: Fluid flow at peripheral section and center section of helical static mixer (Noritake, n.d.).

So, if it is viewed from the cross section of the pipe this flow can be described as a movement that rotates in the semicircular part partitioned by the element, subsequently causing the fluid to spread out along the element. Eventually, the layer of the mixed fluid will become thinner.

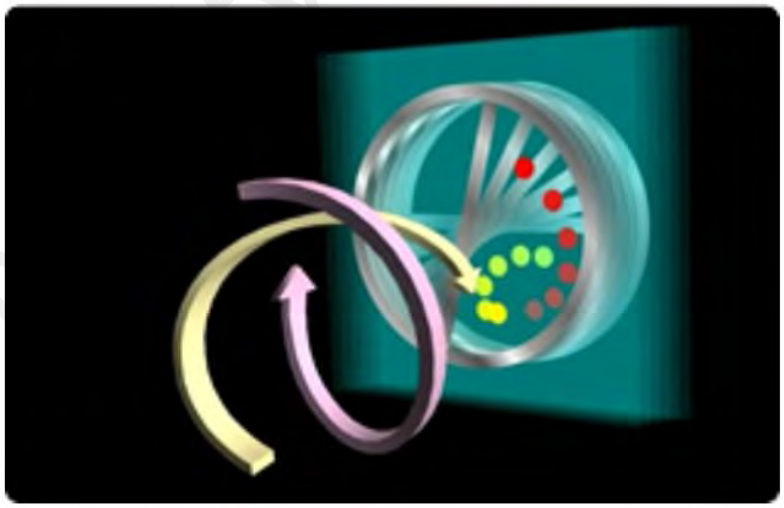

Figure 2.23: Conversion process of static mixer (Noritake, n.d.)

Meanwhile, inversion process also takes place inside the static mixer. The rotation direction of liquids varies in each element, causing the inertial force to be inversed abruptly, which agitates the liquid. The reversed functions work in such way that the fluid is first induced into his clockwise turning flow during its passage through the element has its flow reversed counterclockwise by the following element and the processes continue until the last element.

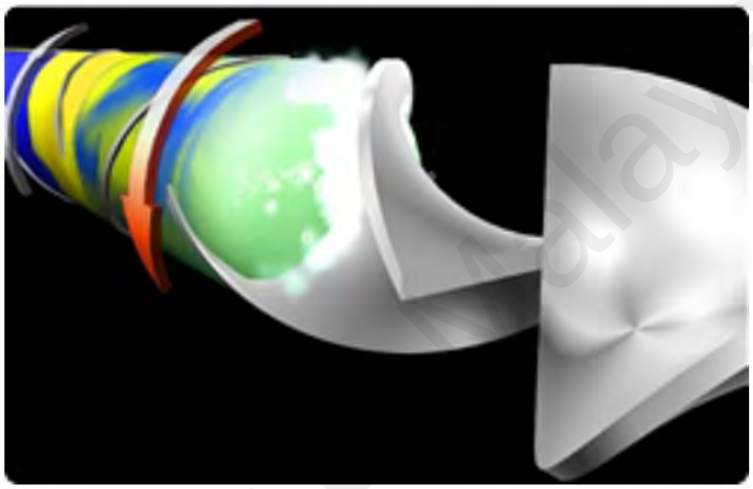

Figure 2.24: Inversion process in static mixer (Noritake, n.d.).

2.3.1.8 Porous Method

From the studies conducted by Kukizaki and Goto (2006), monodispersed nanobubbles or microbubbles inside the aqueous solutions can be generated by using Shirasu porous glass (SPG) membranes with the aid of surfactant addition. Moreover, a few factors were examined for this porous method, such as physicochemical properties of the fluids and physicochemical properties of the membrane. Also, membrane hydrophobicity, symmetry or asymmetry of the membrane and the pore size of membrane are categorized as physicochemical properties of membrane whereas addition of different types of surfactants, viscosity and surface tension are grouped under physicochemical properties of the fluids.

It was noticed that a linear correlation exists between the pore diameters of membrane (43, 55, 64 and 85nm) and sizes of bubble (from 360 to 720nm). The small bubbles were generated under a liquid crossflow in sodium dodecyl sulfate (SDS) solution (0.3%) with ratio of transmembrane pressure (TMP)/bubble point (BP) equals to 1.1 using a tubular SPG membrane. Next, similar trend was observed when tested with flat SPG membrane in different surfactant solutions using same TMP/BP ratio.

Secondly, it is also important to study the membrane hydrophobicity because it will influence the size of bubbles. It can be identified via the water droplet contact angle that drops on the surface of membrane. When the contact angle is higher than 90°, water will be introduced with pressure into the pores and the membrane is known as hydrophobic. On the contrary, when the contact angle less than 90°, membrane pores will be entered by water spontaneously. It is because the force that contracts the contact zone between the membrane and bubble is lesser than the force expanding the bubbles and bubble expands better with a higher contact angle. Therefore, to generate smaller size bubbles, the pores and the surface of membrane must be very hydrophobic, and the surface of the membrane must be treated to decrease the water contact angle value.

On the other hand, Kukizaki (2006) stated when the bubble diameter/ membrane pore diameter equals to ratio of 9, a uniform microbubble was formed in sucrose laurate solution (1%) using asymmetric SPG membrane when a TMP/BP ratio equals to less than 1.5 was implemented, with applied gaseous fluxes. It was observed that asymmetric membrane will encounter 40 times higher of gaseous fluxes than symmetric membrane under the situation where the TMP/BP ratio equals to 1.5. This is due to the reason that the asymmetric membrane has lower hydrodynamic resistance as it operates only with one filtration layer placed at the internal tube surface. Moreover, the lower the thickness of membrane skin layer, the higher the proportion of active pores. Hence, in order to

provide uniform microbubbles and improve the gas fraction, asymmetric membrane and low TMP/B ratio must be used.

Furthermore, it is also important to study the surface tension effect as it has a great relationship with the size of microbubbles. From the research of Kukizaki and Goto (2006), SPG membrane (pore size of 55nm) with a lower surface tension was observed when surfactant was added in, under a liquid crossflow. There was a trend of decreasing surface tension, varying from 67.4 to 58.0 $mN.m^{-1}$ as bubbles generated in SDS solutions (0.01 to 0.5%). Owing to the reduction of capillary force, the diameter of microbubbles decreases when surface tension reduces. When the capillary force encountered a reduction, the bubble will be kept attached to the pore for a shorter period which causes the formation of smaller size bubbles.

Kukizaki and Goto (2007) had researched on the liquids that contained 0.3% SDS and concentrations of polyethylene glycol (PEG) which were different to determine whether the ratio of air viscosity/liquid viscosity affect the size of bubble. They found out when the bubble viscosity of the liquid increases, the bubble size increases, which can be deduced that the rising of viscosity will actually delay the detachment of the microbubbles.

2.3.2 Challenge of Microbubbles Generation

It is wrong to expect to form microbubbles by blowing the bubbles through small aperture and to assume that smaller aperture would be ideal to generate microbubbles correspondingly small. There are number of challenges to support this statement. First, "anchor" will be formed when the liquid attached to the perimeter of the aperture, as a result of growing bubble attached by wetting force to the solid surface when a bubble is generated from a single aperture (Bandulasena et al, 2008). The bubble will continuously grow until the anchoring restraint on the bubble is exceeded by the buoyant force on the bubble, and then breaks off. So, the bubbles will be broken off by the force balance at a size an order of magnitude larger than the diameter of the aperture due to the low pressure offset scenario.

In addition, it is critically important to take into consideration of the wetting properties of the solid surface. If the surface is hydrophobic, a second anchor force with wider area will be created by the gas phase of the growing bubble as the bubble contact a greater region surface than the aperture perimeter. Then, buoyant force will be increases and greater bubble volume will be needed to overcome it. However, this attractive force is no longer present if the surface is hydrophilic.

Next, due to the spacing between bubbles is irregular and the polydispersity of bubble sizes, larger bubbles tend to form from small apertures and result in quick coalescence of the bubble cloud. The coalescence characteristic will further disrupt the small bubble rapidly even there is a formation of it, which contributes to one of the downsides of using small apertures to generate microbubbles (Bandulasena et al, 2008).

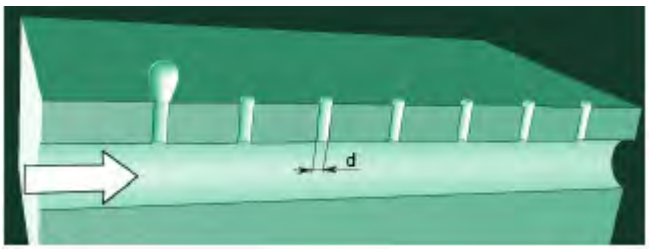

Figure 2.25: Instability of parallel percolation. (Bandulasena et al., 2008)

Moreover, the reason to not form microbubbles through small apertures is parallel percolation becomes unstable when the bubbles are channeled through a porous ceramic material or a nozzle bank. A least resistance path is created by the largest bubble and it will interrupt the growing of the rest of the bubbles in the parallel percolation process. Figure 2.24 indicates that the growth of bubbles becomes easier when one of the bubbles increases to a point beyond the hemispherical shape. So, the lower pressure difference will be overcome as air entering which then induces the growth of the largest bubble, but other bubbles are neglected. This phenomenon is called Young-Laplace surface tension law, where the pressure difference across the water or air surface decreases when the curvature radius *r* increases, as shown in Figure 2.24.

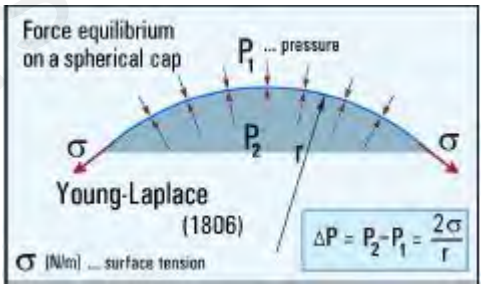

Figure 2.26: Young-Laplace surface tension law. (Bandulasena et al., 2008)

2.4 Microbubbles Measurement Methods

The quantification of microbubble is essentially important to determine the impact that microbubble can bring to the environment. There are few methods being implemented to measure the size of microbubbles because bubbles with smaller size able to stay inside the water for longer time, which is very effective especially for the application of water treatment. For instance, visualization method, laser diffraction and particle image velocimetry.

2.4.1 Laser Diffraction

Laser diffraction or scattering method has been widely used nowadays as the measurement time is shorter and the measurement range is wide and the ease of operation. The main element of this method is the laser beam, where the laser beam will cover the microbubble. Then, the size of the bubble can be determined from the generated scattered light by using spatial intensity distribution pattern (Tsuge, 2016).

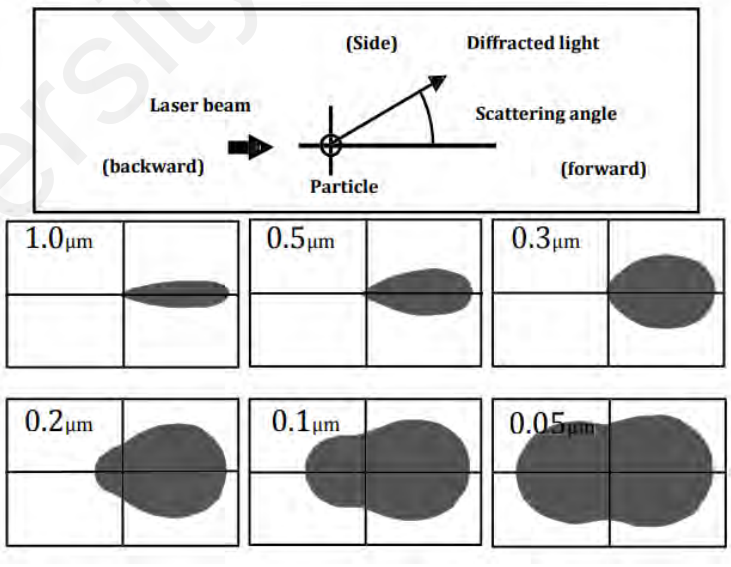

Figure 2.27: Laser diffraction for microbubble measurement (Tsuge, 2016).

The measurement principle is based on the intensity distribution pattern of spatial scattered light when emission of scattered light from particles occurs as microbubbles are exposed to laser beam. Moreover, the scattered light intensity increases when the scattering angle increases, and it indicates changes in particle size. For example, the emission angle of scattered light becomes larger when particle size is smaller and the intensity of light that scatters at the backward of the smaller particle is stronger (Couto et al., 2009). In other words, the intensity of diffracted light increases as the particle size decreases. Since the light intensity of the scattered light differs across various particle size, it is possible to plot the distribution pattern of the light intensity and thus specifying the particle size.

2.4.2 Visualization Method

In addition, the microbubble size can also be estimated through visualization method by means of using naked eye to observe water condition and measure the time taken for bubbles to reach to the water surface. According to PUREBBLE (n.d.), transparent water will turn to be milky color when the generated microbubbles fulfill few criteria, such as the size of bubble ranges from few ten micron to few hundred microns, the quantity of bubbles must be five hundred thousand bubbles/cc (50millions/L) and above. So, the time taken for milky color water to turn to become transparent can be recorded to obtain the bubble rising time from bottom to water surface and the velocity of bubble can be calculated by using:

$$v = \frac{s}{t} \tag{6}$$

where s is the displacement of bubbles to move from bottom to the water surface inside a container, t is the time taken for bubble to rise to water surface and v is the velocity of bubbles. Hence, the size of bubbles can be calculated:

$$v = \frac{\rho_p - \rho_m}{18\mu} g d^2 \quad (7)$$

$$d = \sqrt{\frac{18\mu v}{g(\rho_p - \rho_m)}} \quad (8)$$

where v is bubble velocity, μ is the dynamic viscosity of water, ρ_p is the density of particle, ρ_m is the density of the medium, g is the gravitational acceleration, and d is the diameter of the air bubble.

2.4.3 Particle image velocimetry (PIV)

Particle image velocimetry, or in short form called PIV, is a non-intrusive optical measurement method that applied to develop the image of particle in graphic representation. It operates by injection of seeding particles in the liquid and involve movement of the seeding particles with local flow velocity. Then, the process proceeds with illumination of the seeding particles by light sheet and two successive instants images for the illuminated seeding particles that are suspended in the liquid will be recorded and captured when they move from one place to another (Fouan et al., 2015).

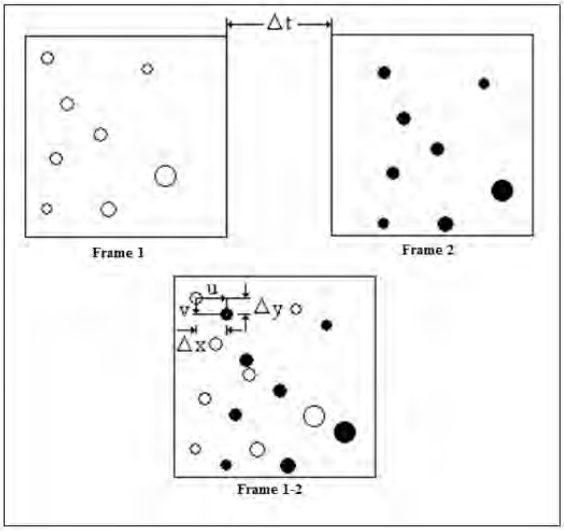

Figure 2.28: Velocity of tracer particles using graphic representation (Fouan et al, 2015).

These two successive instant images will be combined and undergo post processing to obtain the displacement of particles at a certain time interval. This time interval is referring to the time interval between the two captured images within the measurement plane. These data are then used to analyzed and scaled accordingly to obtain the velocity of the particles. The velocity is obtained by interpreting the seeding particles displacement in two consecutive frames and divide it by the time difference between these two consecutive frames.

2.5 Fluid flow of geometry

When the force of air is attached to a solid surface (no-slip boundary condition), especially moving objects like airplanes and automobiles, a resistance or drag force is generated. Besides, pressure drag is induced when flow separation occurs which further increase the resistance to moving objects. This phenomenon occurs when the shape of the moving objects is encountered with abrupt change and that change does not allow the fluid to respond in flow direction, thus stays with the boundary.

So, the boundary layer is separated from the body, then low pressure turbulence region or wake is formed below it. However, wake region only happens when the Reynolds number is large or the object experiences turbulent flow (Batchelor, 1967). The value for Reynolds number with turbulent flow differs for different geometries such as flat plate, circular cylinder or sphere.

Geometry indeed can affect resistance to flow depending how energy losses are incurred and whether they are recoverable or unrecoverable losses. When water flow through a geometry, the fluid must either speed up or slow down as water is incompressible fluid and the continuity of mass flow rate through a conduit of changing cross section needs to be maintained.

$$\dot{m} = v_1 A_1 = v_2 A_2 \tag{9}$$

Since energy must also be conserved

$$P_1 + \frac{1}{2}\rho v_1^2 = P_2 + \frac{1}{2}\rho v_2^2 \tag{10}$$

The P's are the respective pressures or potential fluid energy (pressure) at section 1 and 2, whereas the second term is known as the fluid velocity or kinetic energy. The resistance to flow is

$$R = \frac{P_1 - P_2}{v_2 A_2} \tag{11}$$

The pressure loss is said to be recoverable since the pressure loss can get back to the original static pressure by modifying the conduit. However, there are unrecoverable losses that are not caused by the changes in inertia but rather friction, but in terms of fluids, viscosity.

Viscosity fluid losses turn kinetic energy into heat and the heat can either raise the temperature of the fluid (an internal energy) or escape through the fluid conduit boundaries. Viscous losses normally occur when fluids drag along conduit boundary layers, layers within the fluid itself or when higher dimensional flow occurs (turbulence, vorticity).

Water indeed is a viscous fluid so as the surface area increases, the chance for more drag and energy loss which increases resistance to flow increases, but by a different mechanism. The resistance due to viscous loss would be:

$$R = \frac{Kh^3 b}{12\eta l} \tag{12}$$

2.5.1 Spherical shape

For a sphere shape material, the Reynolds numbers will influence the drag coefficient significantly. In order to understand these changes, it is advised to refer to the details of flow past a cylinder because the 3-dimensional flow past a sphere can be represented by a 2-dimensional flow past a cylinder as they are very similar in term of flow pattern. Also, 2-dimensional flow is easier to be computed and to understand as the dimensionality has been reduced (NASA, n.d.). The fluid flow passes through a sphere and a cylinder through a few transitions corresponding with velocity are shown in Figure 2.28.

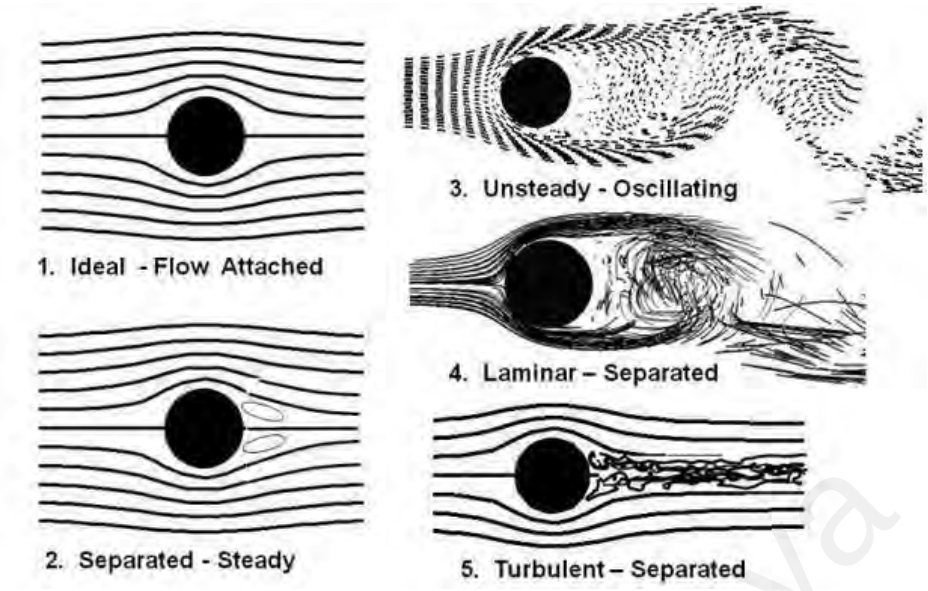

Figure 2.29: Flow past a sphere (NASA, n.d.).

An ideal flow has no boundary layer along the surface, neither separation nor viscous wake at the downstream of the sphere. The viscosity is neglected entirely as the ideal flow has a very slow flow. Owing to the flow is symmetric from upstream to downstream, drag is not encountered on the sphere and it is known as d'Alembert's paradox. Though the viscosity neglection has helped to simplify the analysis process, however, this kind of flow is impossible because viscosity is always present in any fluid even with very small amount.

In addition, at low velocity of flow or steady flow case, downwind side of the sphere will form a stable pair of vortices. High drag is generated by the vortices on the sphere when the steady flow is separated. A flow is considered unsteady flow when the velocity increases, low stability occurs at downstream vortices, with separation occurs and the vortices are alternately shed downstream. At this point, the wake is very wide, and it will induce a huge amount of drag and shedding happens alternately at the downstream Karman vortex sheet.

Apart from that, as the flow velocity increases, vigorous wake can be observed at the back of separation point. Laminar flow always occurs where the boundary layer is thinner than other flow cases and the wake is narrow compared to unsteady periodic flow which leads to a low drag force (NASA, n.d.).

As the flow further increasing the velocity and the Reynold number is found to have exceeded 400,000 when turbulent flow occurs. The separation point moves slightly downstream compared to the separation point of laminar flow, which in turns reducing the drag as the wake is relatively smaller compared with laminar flow.

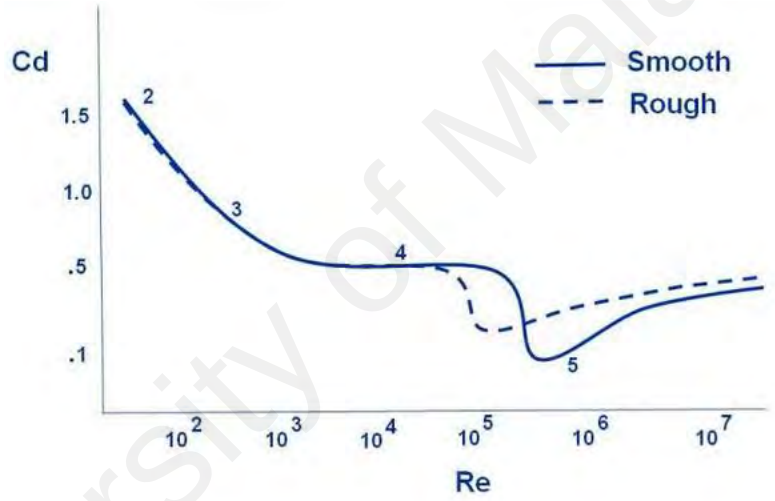

Figure 2.30: Drag of sphere at different Reynolds number (NASA, n.d.).

CHAPTER 3: METHODOLOGY

The research methodology chapter will describe the design of microbubble generator and the design of different air-mixers geometry in details. Also, the instruments and the measurements method that used to record the data will be explained in this chapter.

3.1 Static mixer

The static mixer, as shown in figure 3.1 was selected to be used to generate microbubble. It is made of UPVC, which is of low cost but capable to cater for low energy blending especially water and air particles. Internal part of the static mixer comprises of multiple helical mixers that act as a blender to continually dividing and recombining flow streams such as water and air. The advantages of using static mixer are its flexibility in meeting the requirement of different flow rates application, low maintenance fee, no moving part as static mixers remain motionless during the process of mixing and ability to achieve optimum mixing status in various difficult flow conditions.

The operating principle is that the precisely configured static mixer will shear the water and air bubbles into smaller components when they enter the mixer. What drives the mixer works effectively is the flow division mechanism, where the helical elements are well arranged in a series configuration of alternating right and left hand 180 twisting degree (Lenntech, n.d.). When air bubble and water first flow into it, the helical mixer will split the mixing components into two streams and rotate them through 180 degrees. The layer thickness decreases as the number of layers or streams increases. In other words, the mixing capability is also depending on the number of elements.

Figure 3.1: Static mixer.

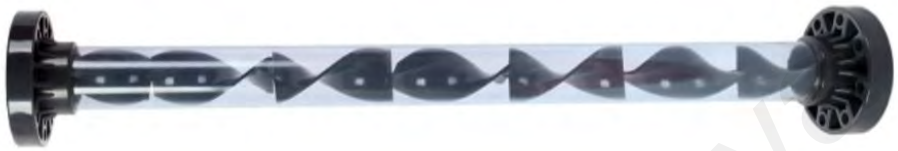

Figure 3.2: Internal structure of static mixer.

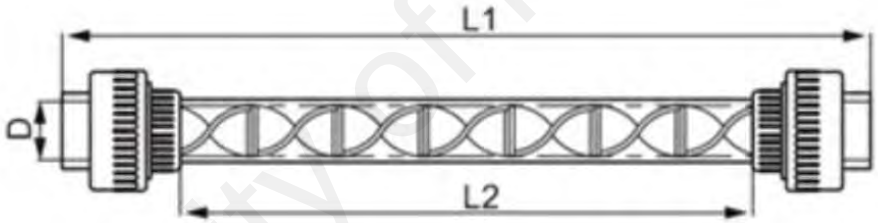

Figure 3.3: Static mixer drawing.

3.2 Experimental Setup

The first stage of conducting the experiment is to prepare the layout, instruments and materials needed such as water pump, PVC pipe, venturi, static mixer, pressure gauge, valve, air meter, dissolved oxygen (DO) meter, etc. First, design of the microbubble system was sketched prior to the procurement of materials because it gave a clear idea of the bill of material so that the cost spend is within planned budget. The schematic diagram of the microbubble system is shown in figure 3.4.

A big water tank (88cm x 56cm x 19.5cm) was prepared and the check valve is dipped inside the water. Normal water pump of 0.75kW, 1hp was used to suck the water from water tank and supply for microbubble generation. The check valve was connected to the water pump via T-joint and a pressure gauge was placed after the water pump to monitor the pressure of the water.

Then, venturi with air meter and ball valve were installed at the T-joint right after the pressure gauge, P1 and the ball valve served as a bypass valve. Another pressure gauge, P2 will be placed in between the spherical marbles and venturi to record the pressure of water after venturi. Apart from that, static mixer was connected to the spherical marbles and pressure gauge, P3 was installed to collect pressure after the static mixer. Finally, a ball valve was fitted to allow the control of the flow of water at the outlet of nozzle.

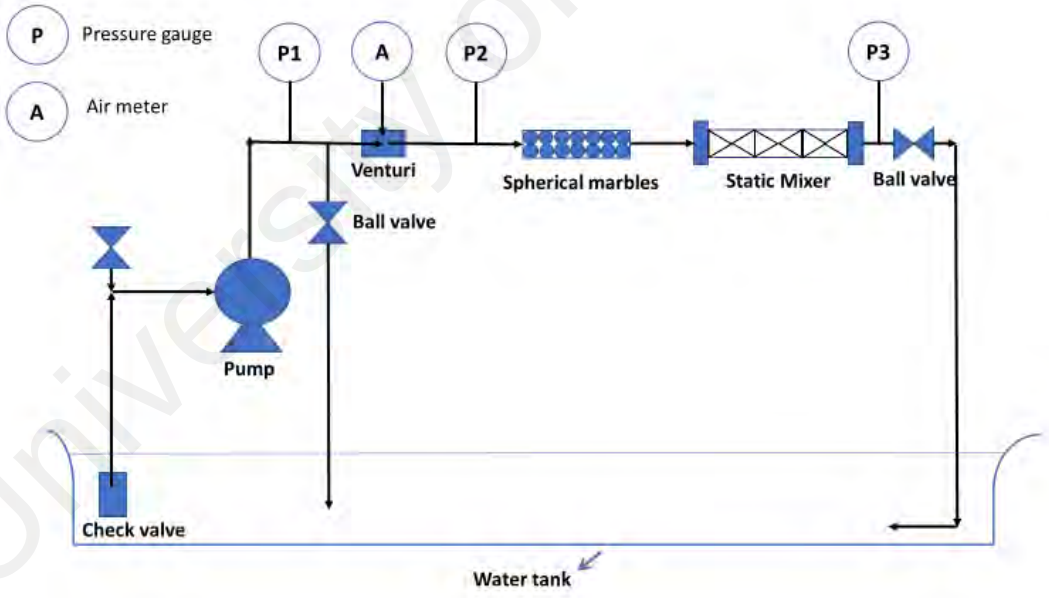

Figure 3.4: Schematic diagram of microbubble generator.

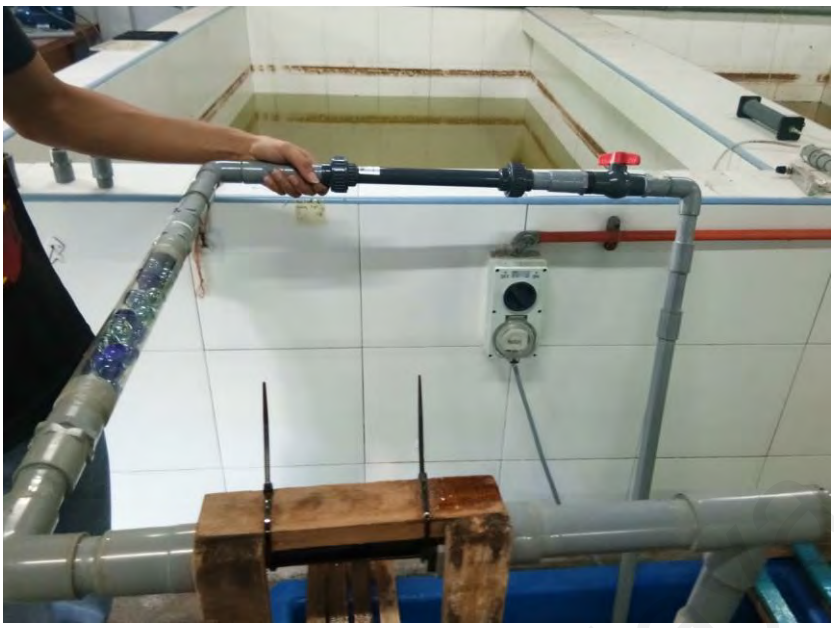

Figure 3.5: Setup of microbubble generator.

3.2.1 Individual System

The microbubble generation system comprises of different types of equipment and instruments. For instance, high pressure water pump that can supply up to 8 bars is used in this research project to suck the water from water tank and mix with the air and circulate back to the water tank.

Next, venturi as a key element in this project is implemented to serve as a air supply air mixing agent where it operates to allow air suction to take place when water pump performs water suction along the pipeline system. Check valve is another fitting that used to provide one-way flow when water is being sucked from water tank by the water pump as shown in figure 3.6. There are few types of fitting used to fabricate the pipeline of this microbubble generation system, such as elbows, tee, valves, connector and PVC pipe. The size of the pipe fittings is 15mm with class 6 material to withstand high pressure of the water during suction.

Figure 3.6: Check valve.

In order to measure the reading of the air supply, air meter is implemented with the capability to measure the air flow rate ranges from 0 to 10 L/min as shown in **Figure 3.8**. The air meter is connected to the inlet of the venturi as the air suction occurs at the inlet of the venturi.

Figure 3.7: Air meter

Furthermore, pressure gauges are installed in the pipeline system to measure the pressure of the water at different regions when water passes through it. By doing that, the pressure difference can be calculated and any pressure losses in the water can be recorded. Dissolved oxygen (DO) meter is applied to obtain the DO reading for the specimen taken from the water tank.

Figure 3.8: Pressure gauge.

Figure 3.9: Measuring cylinder (100ml).

As shown in Figure 3.9, measuring cylinder is used to estimate and observe the bubble conditions inside the water. The water sample that contained tiny bubbles will be filled into this measuring cylinder and observation and recording will start to understand the microbubble conditions and estimate the time taken for bubbles to rise from bottom to the water surface

3.2.2 Dispersing Elements Drawing

There are two types of dispersing elements used, which are single-phase marble elements and two-phase marble elements. The dispersing elements are in static form which allow the fluid to pass through it and create turbulence flow to shred the bubbles into smaller bubbles. Moreover, turbulent flow is very effective for mixing process as it has eddy viscosity whereby the energy, momentum and heat can be quickly transported from one place to another. So, the eddying motions will smooth out the difference in momentum by molecular interactions thus the mixing is more effective than laminar flow.

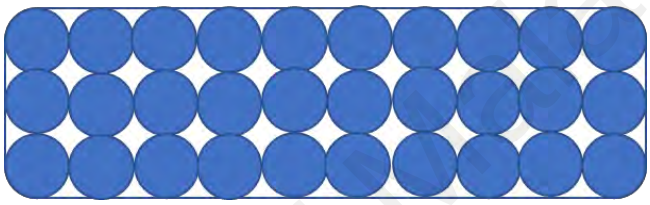

Figure 3.10: Cross sectional view of single-phase marbles.

The design of single-phase marble is plotted in Figure 3.10. The size of the marbles is fixed to 16mm and the is arranged in mannerly order as shown in the cross-sectional view of the drawing. It is placed after venturi to enhance the air mixing and bubbles shredding processes. According to Chen (2016), a swirling spinning motion will be induced as the fluid performs rotary motion, then the negative pressure is generated along the axis as the fluid moves and the air bubble undergoes continuous further cut into tiny bubbles.

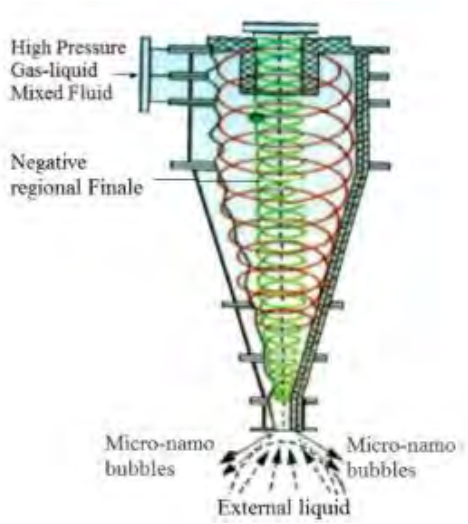

Figure 3.11: Swirling motion of fluid across spherical body (Chen, 2016).

To further improve this concept, smaller size of bubble is introduced into the single-phase marbles to create two-phase flow. In this research study, glass marbles of 10mm are used to replaced half of the 16mm marbles and the new arrangement is as shown in Figure 3.12. It is noticed that the number of marbles is increasing, and this will enhance the water-air mixing process as the fluid will encounter more and more shredding when it moves from 16mm marbles to 10mm marbles. As a result, this will further enhance the swirling spinning motion as well.

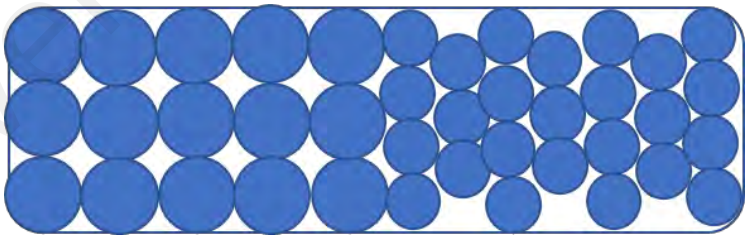

Figure 3.12: Cross-sectional view of two-phase marbles.

3.3 Experimental cases

As mentioned before, there are total of 4 cases that will be tested in this research project. These cases are depicted in Figures 3.13, Figure 3.14, Figure 3.15 and Figure 3.16. For case 1, venturi is used as a main element for microbubble generation. It serves for air suction purpose and improve the process of water-air mixing by inducing cavitation to enable instantaneous mixing to create thousands of minute bubbles. Besides, the ball valve after P3 is used to control the pressure of the fluid flow of the pipeline system. Air meter is installed on top of the air inlet of venturi to measure the inlet air flow rate.

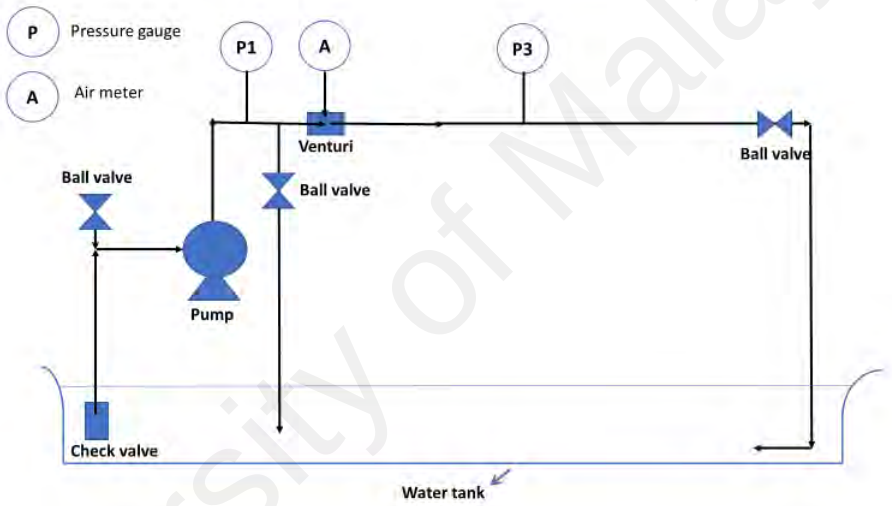

Figure 3.13: Venturi (Case 1).

Next, a static mixer is added to the venturi system to create another case, which is case 2. Static mixer operates in such a way that it involves three major processes, namely division, conversion and inversion. First, the fluid will be split into half as it passes through the first helical shape element. Conversion occurs at the wall of cylinder and center part, where the liquid at cylinder switches to center and liquid at center part switches to cylinder wall. Eventually, inversion process takes place when the direction of fluid movement keeps changing as it passes through each element which will enhance the agitation of liquid as the inertia force is being induced along the liquid rotation inside the static mixer.

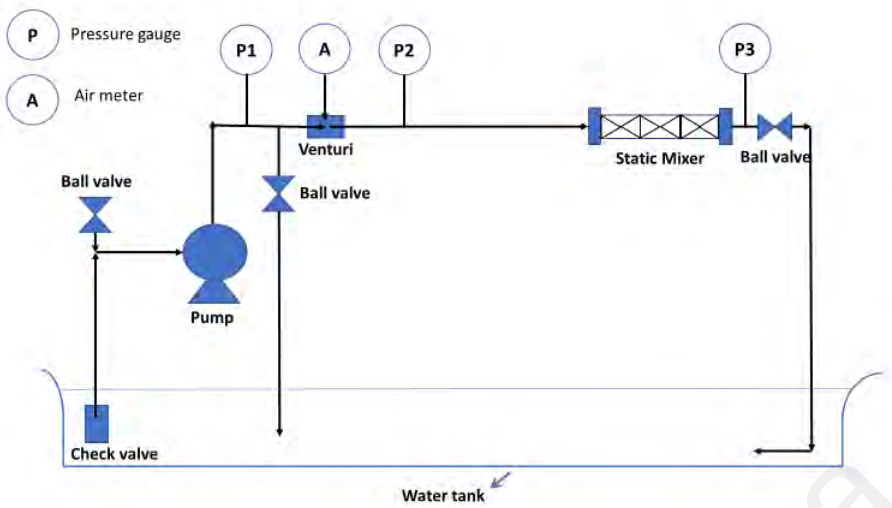

Figure 3.14: Venturi and static mixer (Case 2).

Moreover, a cylinder that filled in 16mm marbles or single-phase marble elements are connected to venturi and static mixer in case 3. The spherical design of the marbles is arranged in a cascade form because when the fluid passes through the first spherical element, turbulence will be induced due to the capability of pump that can generate strong water flow. The cascaded design will cause the wake produced by the first spherical element to be disturbed and the subsequent incoming fluid will force the wake resulted from previous fluid to move towards the moving axis. Hence, a strong agitation occurs repeatedly such that the air bubbles will be separated into smaller bubbles and mixing process is optimized.

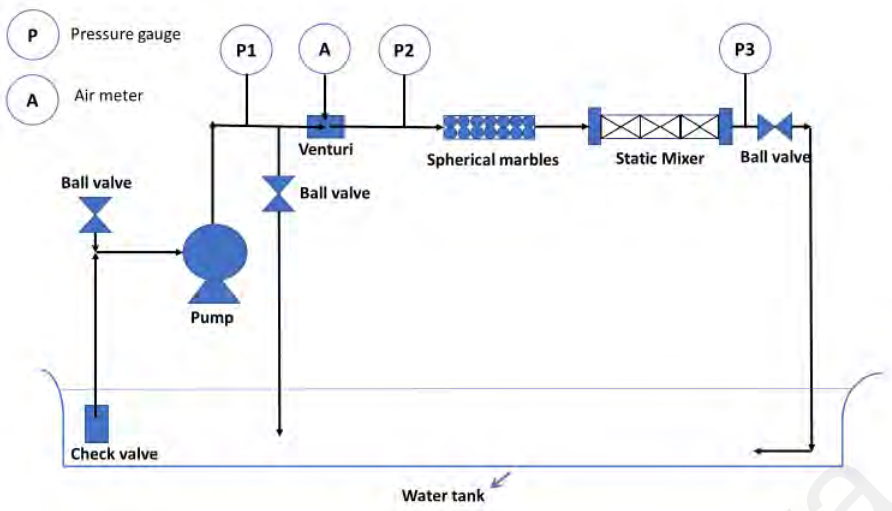

Figure 3.15: Venturi, single-phase marbles and static mixer (Case 3).

Apart from that, the single-phase marbles are taken out from the pipeline system and replaced with a modified version called 2-phase marbles in which half of the 16mm marbles are replaced with 10mm marbles, as shown in Figure 3.16. The 2-phase marbles are capable to generate even stronger agitation inside the marbles as the fluid disperse. It can be noticed that the pores in between the marbles become even smaller that the fluid is forced to squeeze in through the elements inside. Hence, the fluids that are waiting to pass through these constricted regions will hit by the new incoming fluids, thus generating smaller bubbles size and enhance dissolution of oxygen.

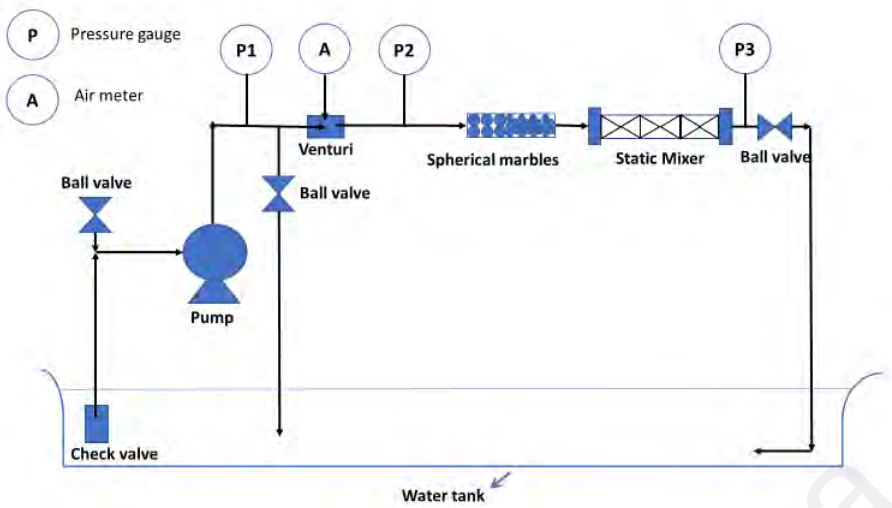

Figure 3.16: Venturi, two-phase marbles and static mixer (Case 4).

3.4 Experimental Procedures

The work flow of the microbubble generator is shown in Figure 3.17. First, the water tank was filled with water until 70% full. Then, the fittings, measuring instruments, supports, static mixer, spherical marbles were setup. The piping system was ensured connected properly and wrapped with seal tape to prevent water leaking and causing any pressure losses. When the setup was completed, the water pump was turned on and water will be sucked through the check valve in one-way flow and passed through the water pump. Next, the second ball valve at stage 3 operated as a bypass function where it helped to reduce the water pressure and the data with bypass system was collected and presented in the next chapter. Meanwhile, venturi will start to suck the surrounding air according to Bernoulli's Principle, the air flow condition will be shown in the air meter. This is also where the air bubbles started to mix with the water to create microbubbles.

The mixture of air bubbles and water will further pass through the spherical marbles and water particle will be sheared off to further enhance the mixing of air bubbles and water. Moreover, another stage of break-off of air bubbles to smaller size will occur at static mixer. It was where the mixing of air bubbles and water started to optimize, and microbubbles formed after several dividing and mixing stage.

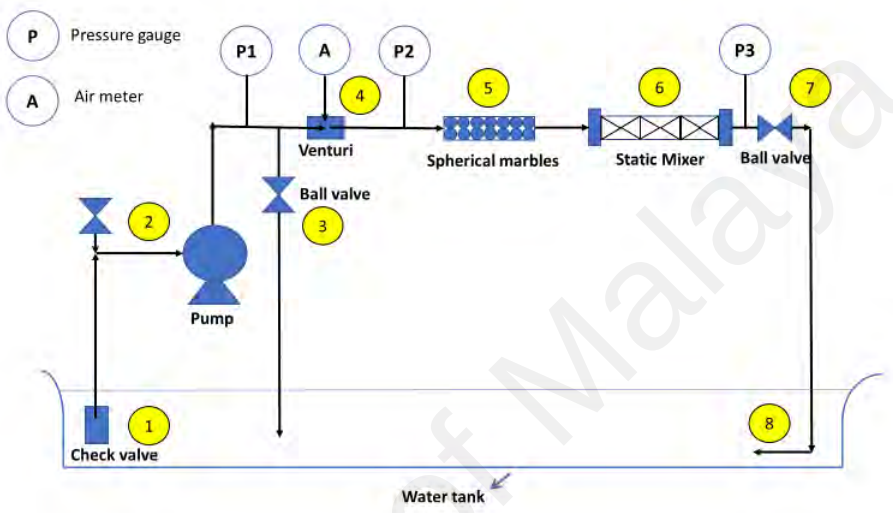

Figure 3.17: Work flow of microbubble generator

Finally, water-air mixing components will pass through the nozzle at stage 8 and disperse to the water tank and the process of microbubble generation continued in a cycle manner. The ball valve at stage 7 acted as a gate to control the overall water pressure and the water quality at pressure of 0.4 bar, 0.8 bar, 1.2 bar, 1.6 bar, 2.0 bar, 2.4 bar, 2.8 bar, 3.2 bar and 3.4 bar were collected together with their respective pressure at P1, P2, temperature, air flow rate and time taken for the bubble to rise to the water surface of a measuring cylinder. The above steps and data collection were repeated for another 3 cases, total of 4 cases which are:

1. Venturi
2. Venturi with static mixer
3. Venturi with static mixer and single-phase marbles
4. Venturi with static mixer and 2-phase marbles

The bubble size can be calculated from the bubble rising time by using terminal velocity equation from Stokes' Law (911Metallurgist, n.d.),

$$v = \frac{\rho_p - \rho_m}{18\mu} g d^2 \tag{13}$$

Rearrange the formula will get:

$$d = \sqrt{\frac{18\mu v}{g|(\rho_p - \rho_m)|}} \tag{14}$$

where v is bubble velocity, μ is the dynamic viscosity of water, ρ_p is the density of particle, ρ_m is the density of the medium, g is the gravitational acceleration, and d is the diameter of the air bubble. The velocity of air bubbles was calculated by using:

$$v = \frac{s}{t} \tag{15}$$

where s is the travel distance of air bubbles and t is the time for bubble to rise to the surface of water. In this study, a 100ml measuring cylinder was used to contain the microbubbles water which was in milky look and time taken for bubbles to fully reach 100ml was recorded. In other words, time taken for milky water to turn to transparent was recorded. The height of the measuring cylinder from 0ml to 100ml is 24cm or 0.24m and the bubbles velocity was calculated by diving the height by bubble rising time.

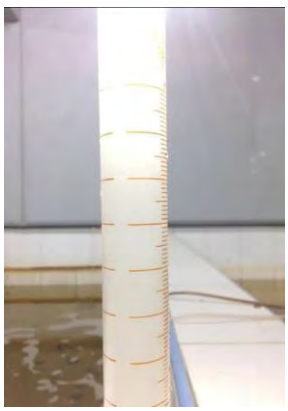

Figure 3.18: Microbubbles state of water with milky or cloudy look.

Sample calculation for bubble diameter is shown as below:

For Case 1,

P2: 0.40 bar

Temperature: 34℃

Gravitational acceleration: 9.81 m/s^2

Dynamic viscosity, μ at 34℃: $7.34 \times 10^{-4} Ns/m^2$

Velocity, v1: $5.3 \times 10^{-3}\ m/s$

Density of Oxygen, O_2 : 1.41 kg/m^3

Density of Water, H_2O : 1000 kg/m^3

$$d = \sqrt{\frac{18(7.34 \times 10^{-4})(5.3 \times 10^{-3})}{9.81|(1.41 - 1000)|}} = 85\ \mu m$$

CHAPTER 4: RESULTS AND DISCUSSION

4.1 Bubble Rising Time and Bubble Size for Different Cases

The rising time for bubbles varied when tested with different configuration as pressure 2, P2 was having various settings such a way that each time the new setting was increased by 0.4 bar compared to previously setting. Started with pressure equalled to 0.40 bar, followed by 0.80 bar, 1.20 bar until a point just before the water encountered backflow and flow out from the air suction point of venturi, which was 3.40 bar. The bubble rising time for different cases were plotted in table 4.1.

Table 4.1: Bubble rising time for different cases

No	P2 (bar)	t1 (s)	t2 (s)	t3 (s)	t4 (s)
1	0.40	45.00	74.00	77.00	75.00
2	0.80	50.00	72.00	77.00	81.00
3	1.20	54.00	73.00	76.00	81.00
4	1.60	60.00	75.00	80.00	84.00
5	2.00	61.00	83.00	76.00	84.00
6	2.40	65.00	82.00	82.00	83.00
7	2.80	20.00	86.00	86.00	88.00
8	3.20	30.00	89.00	96.00	91.00
9	3.40	43.00	85.00	96.00	102.00

Table 4.2. List of cases

Case	Description
1	Venturi
2	Venturi + Static Mixer
3	Venturi + Static Mixer + Marbles
4	Venturi + Static Mixer + 2 Phase Marbles

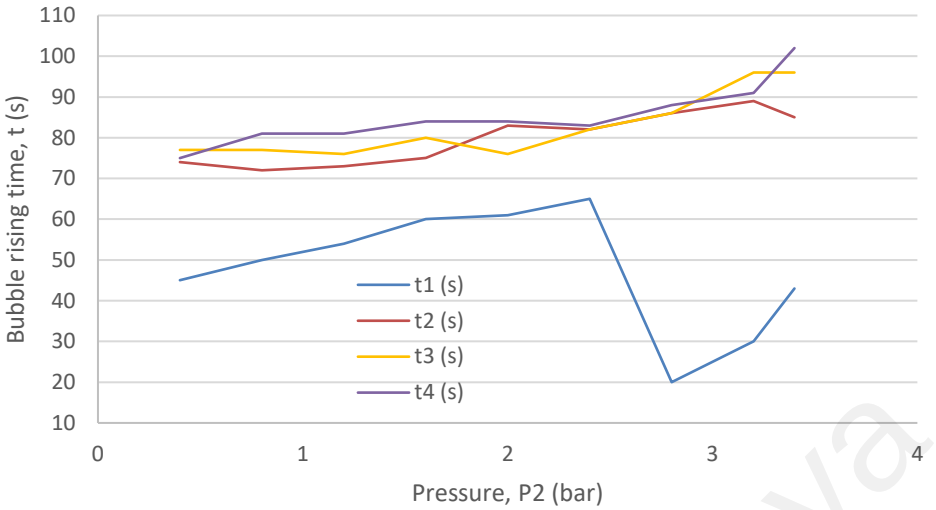

Figure 4.1: Bubble rising time versus pressure.

The data has shown that the bubble rising time for case 1 is the lowest among others. The transition period started after 2.0 bar where the bubble rising time for 4 cases showed different trend. For example, case 1 which is system with venturi only experienced a substantial dropped of bubble rising time and bounce up at 2.9 bar, while the other 3 cases showed insignificant increased of bubble rising time during the transition period. The optimum pressure for highest bubble rising time for case 2, case 3 and case 4 occurred at 3.4 bar while case 1 happened at 2.4 bar.

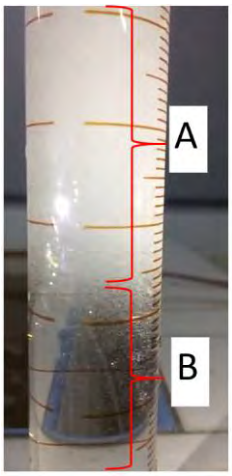

Figure 4.2: Microbubble state and normal state in water.

The condition of water turned into milky or cloudy when the microbubbles mix with water. The microbubbles have a grey milky colour under the best operational condition, which was 3.4 bar. The recording stopped when the water turned into normal (A) or the microbubbles (B) had reached the surface of the water as illustrated in Figure 4.2.

Table 4.3: Temperature, velocity and diameter of case 1.

No	Pressure, P (bar)	Temperature (degC)	Dynamic viscosity (N.s/m^2)	v1(m/s)	Diameter 1 (μm)
1	0.40	34.00	0.000734	0.0053	85
2	0.80	35.70	0.000710	0.0048	79
3	1.20	36.00	0.000706	0.0044	76
4	1.60	37.00	0.000692	0.0040	71
5	2.00	37.50	0.000686	0.0039	70
6	2.40	37.80	0.000682	0.0037	68
7	2.80	37.90	0.000680	0.0120	122
8	3.20	38.40	0.000674	0.0080	100
9	3.40	38.50	0.000673	0.0056	83

From Table 4.3, the smallest bubble diameter, 68 μm obtained was at 2.4 bar when the bubble rising velocity was at 0.0037 m/s, which is the slowest amongst others. Meanwhile, the biggest bubble diameter was found right after 2.4 bar, which was 122 μm at 2.8 bar which had the faster bubble rising velocity. From the bubble rising velocity trend, it can be said that the bubble rising velocity is a function of bubble diameter for case, where diameter of bubble reduced as bubble rising velocity reduced.

Table 4.4: Temperature, velocity and diameter of case 2.

No	Pressure, P (bar)	Temperature (degC)	Dynamic viscosity (N.s/m^2)	v2(m/s)	Diameter 2 (μm)
1	0.40	33.90	0.000736	0.0031	65
2	0.80	33.70	0.000739	0.0031	65
3	1.20	34.30	0.000730	0.0032	65
4	1.60	34.20	0.000731	0.0030	63
5	2.00	34.20	0.000731	0.0032	65
6	2.40	34.00	0.000734	0.0029	63
7	2.80	34.10	0.000733	0.0028	61
8	3.20	32.90	0.000751	0.0025	59
9	3.40	34.60	0.000726	0.0025	58

Table 4.5: Temperature, velocity and diameter of case 3.

No	Pressure, P (bar)	Temperature (degC)	Dynamic viscosity (Ns/m^2)	v3(m/s)	Diameter 3 (μm)
1	0.40	34.20	0.000731	0.0032	66
2	0.80	34.50	0.000727	0.0030	63
3	1.20	34.30	0.000730	0.0030	63
4	1.60	34.60	0.000726	0.0029	62
5	2.00	34.20	0.000731	0.0029	62
6	2.40	34.40	0.000728	0.0029	62
7	2.80	34.90	0.000721	0.0027	60
8	3.20	34.60	0.000726	0.0026	59
9	3.40	35.50	0.000713	0.0024	56

Table 4.6: Temperature, velocity and diameter of case 4.

No	Pressure, P (bar)	Temperature (degC)	Dynamic viscosity (N.s/m^2)	v4(m/s)	Diameter 4 (μm)
1	0.40	32.70	0.000754	0.0032	67
2	0.80	32.70	0.000754	0.0030	64
3	1.20	33.80	0.000737	0.0030	63
4	1.60	33.90	0.000736	0.0029	62
5	2.00	34.20	0.000731	0.0029	62
6	2.40	34.20	0.000731	0.0029	62
7	2.80	34.40	0.000728	0.0027	60
8	3.20	34.60	0.000726	0.0026	59
9	3.40	34.70	0.000724	0.0024	56

Table 4.7: Diameter of different cases at different pressure value

Pressure, P (bar)	Diameter 1 (μm)	Diameter 2 (μm)	Diameter 3 (μm)	Diameter 4 (μm)
0.40	85	65	66	67
0.80	79	65	63	64
1.20	76	65	63	63
1.60	71	63	62	62
2.00	70	65	62	62
2.40	68	63	62	62
2.80	122	61	60	60
3.20	100	59	59	59
3.40	83	58	56	56

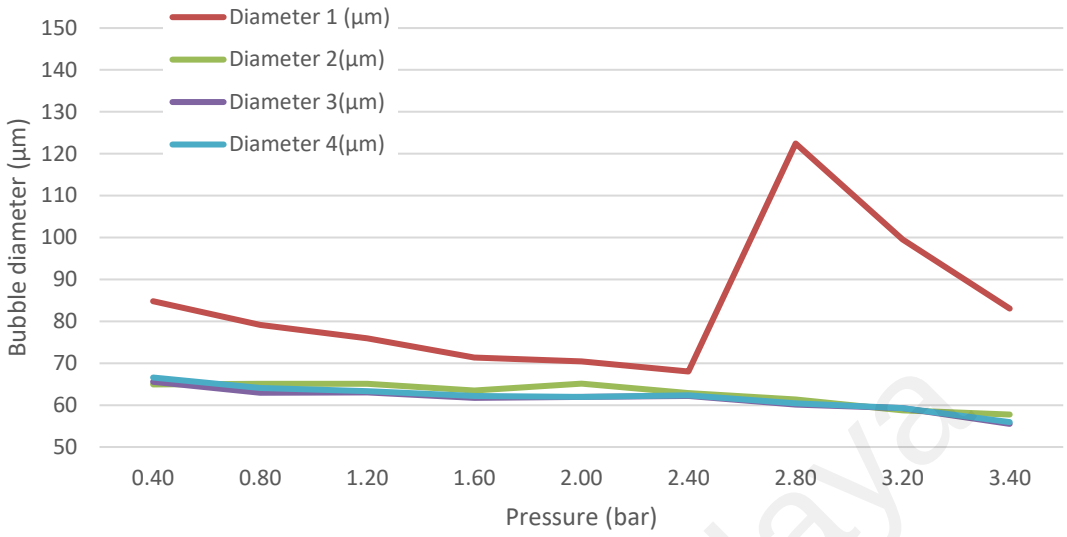

Figure 4.3: Bubble diameter vs Pressure for different cases.

Based on Figure 4.3, the diameter of bubble for case 2, case 3 and case 4 indicated similar trend when the pressure increased from 0.40 bar to 3.40 bar, in which the bubble diameter decreased slightly from an average of 66 µm to 57 µm. In order to reproduce the condition of low pressure in a shallow liquid and high pressure in a deep liquid, the water pressures were varied from lower pressure to higher pressure. Higher pressure indicated greater pressure acted on the bubbles, which will compress the bubble to make it smaller while the force acted on bubble is lesser when the pressure of liquid is lower. Therefore, the rising speed of bubble increased as pressure increased and rising speed is a function of bubble diameter, so the bubble size also acted inversely proportional to the water pressure.

In addition, the bubble diameter with only venturi only yielded 83µm at its optimum setting while the optimum setting for case 2, case 3 and case 4 had further reduced the bubble diameter by around 10µm. It has proven that static mixer has the capability to shred the bubble into smaller size or the adding of static mixer is able to reduce the diameter of bubble by 15%. Furthermore, the implementation of spherical marbles did not help to split the microbubble into smaller size though there were very little diameter reduction encountered in case 3 and case 4. This has also shown that multiple separation phase did not contribute to tremendous impact on the bubble size reduction for the microbubble generator used in this study.

4.2 Dissolved Oxygen (DO) for different cases

In this study, the dissolved oxygen (DO) for 4 cases were recorded and plotted into graphs.

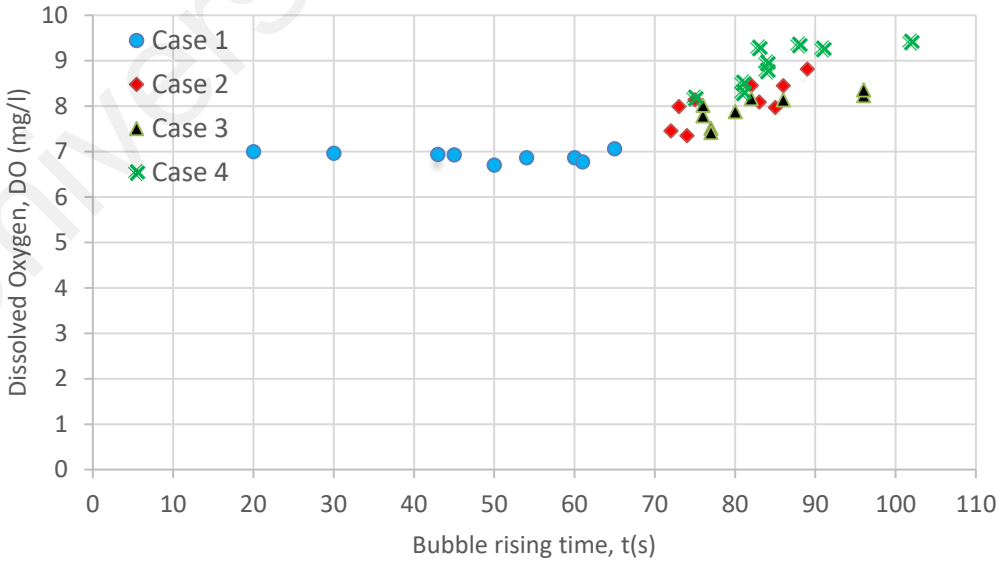

Figure 4.4 DO vs bubble rising time for 4 cases.

Bubble rising time had been compared to the dissolved oxygen in this study and results from Figure 4.4 had depicted the relationship between bubble rising time and DO. When the microbubble generator consists of venturi, the bubble rising time increased from 20s to 65s but the DO remain stagnant all the time. However, there was an increment in the DO value (more than 7.5 mg/L) when static mixer was introduced into the system. When marbles were added to the microbubble generator (case 3), bubble rising time had further improved but DO increment was slightly weaker than case 2. This is because actual amount of dissolved oxygen (mg/L) or the solubility of oxygen relies on the pressure, salinity and pressure (FONDRIEST, n.d.).

Nevertheless, a maximum DO of 9.41 mg/L was recorded when 2 phases marbles were installed. Though temperature is the major contributor to the DO value, the dissolution rate of oxygen is driven by Reynolds number as well (Fee, Grant and Newton, 1976). High Reynolds number plays a vital role in the solubility of oxygen in water, As the water flow reaches turbulence state (Re> 4000), the flow is moving vigorously by visual inspection and stronger wake can be observed when the water flows through spherical object. So, when 2 phases of marbles were implemented, the degree of turbulence increased, which enabled more oxygen to be dissolved inside the water. In other words, dissolution rate of oxygen increases as the wake region becomes stronger or higher Reynolds number is reached.

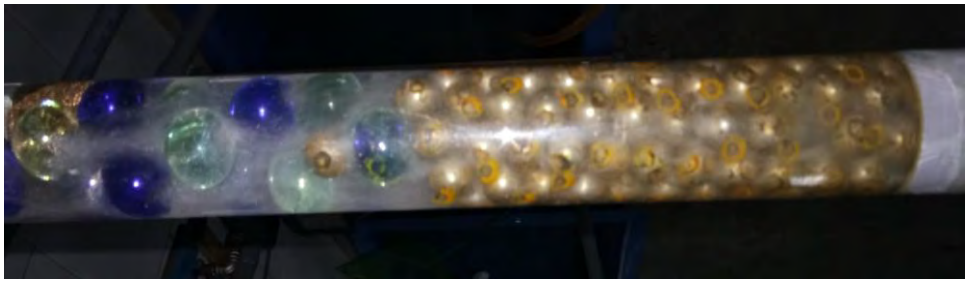

Figure 4.5 Flow condition of two-phase marbles.

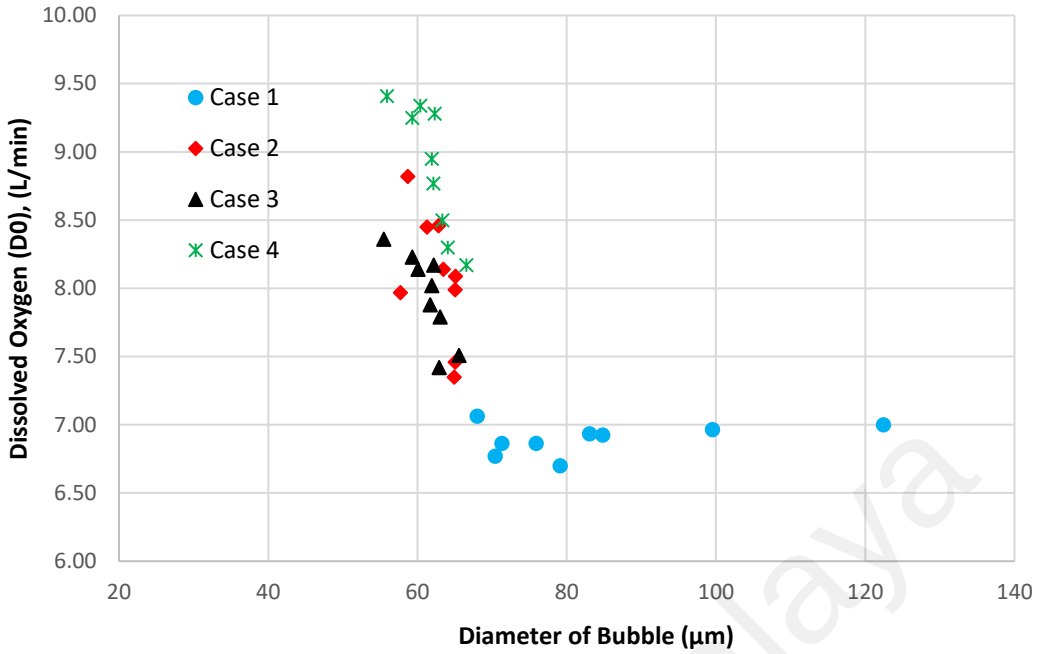

Figure 4.6: DO vs diameter of bubble for 4 cases.

The results obtained from the analysis of DO versus diameter of bubble for 4 different cases are summarized in Figure 4.6. The most interesting of aspect of this graph is the bubble size or diameter has significant effect on the dissolved oxygen (DO) of water. Owing to the large hydrostatic pressure, microbubbles can hold more dissolved oxygen than big bubbles. From the data in Figure 4.6, it is apparent that the DO surged up by around 40% as diameter of bubble decreased by 12%. Having smaller size of bubbles reveal that larger interfacial area per unit volume can be obtained which indicates larger gas dissolution. In other words, when bubble diameter decreases, dissolved oxygen (DO) increases.

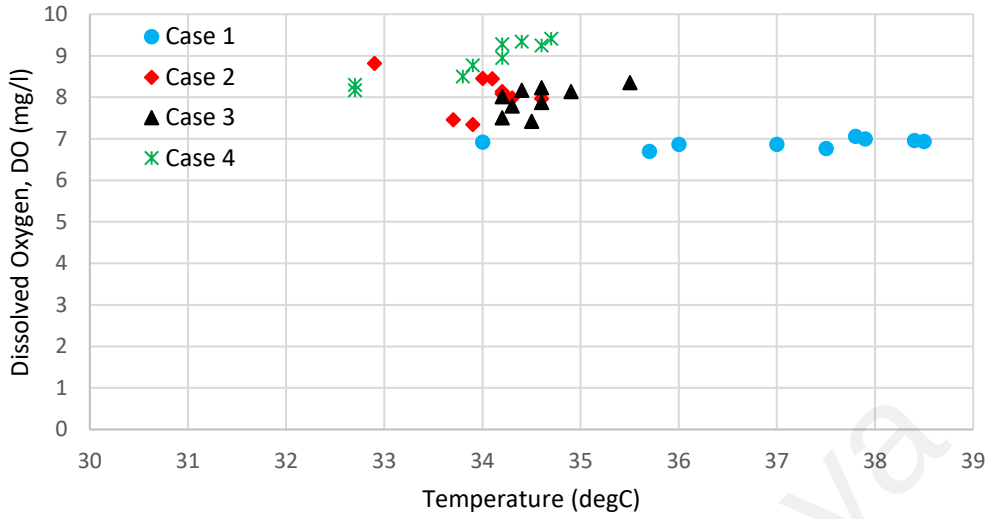

Figure 4.7: DO vs temperature for 4 cases.

According to Bruckner (n.d.), the saturation of oxygen is temperature dependent. Oxygen is more soluble in water with lower temperature and less soluble as temperature becomes higher. For example, at temperature of 15℃, the oxygen concentration of water is around 10.2mg/L while at temperature of 25℃ the oxygen concentration of water is 8.6mg/L. From the graph plotted in Figure 4.7, the dissolved oxygen for 4 different cases were more than 7 mg/L when the temperatures were less than 35℃. The temperature dependent characteristic was proven in case 2 (venturi and static mixer) where the DO obtained was 8.82mg/L when the temperature of water was recorded at 32.9℃. There were two outliers did not follow the temperature dependent trait due to the different pressure setting during the experiment. As mentioned before, the solubility of oxygen does not depend only on the temperature of the medium but the pressure and the salinity of medium. Hence, both case 3 and case 4 did not portray a DO decreasing trend when temperature increased.

4.3 Effect of Pressure vs DO and Bubble Rising Time

In this paragraph, the relationship of pressure versus dissolved oxygen (DO) and bubble rising time will be discussed. The correlation graphs for 4 different cases were plotted as shown below, which are Figure 4.8, Figure 4.9, Figure 4.10 and Figure 4.11. For microbubble system with only venturi, the DO values did not show any significant difference when the water pressure increases. However, the bubble rising time was increasing when pressure of the water was tuned up. The bubble rising time encountered a huge dropped at 2.8 bar and bounced up at 3.2 bar. It can be said that 2.8 bar is the 'sweet spot' which bubble rising time and DO started to decrease right after this 'sweet spot'.

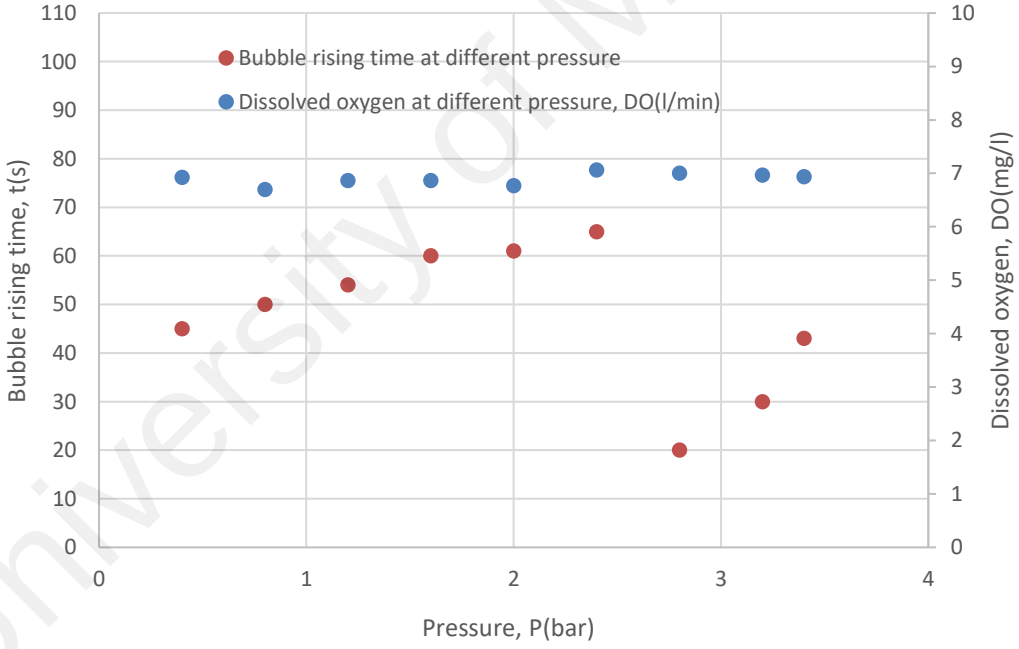

Figure 4.8: Bubble rising time and DO versus pressure for venturi (case 1).

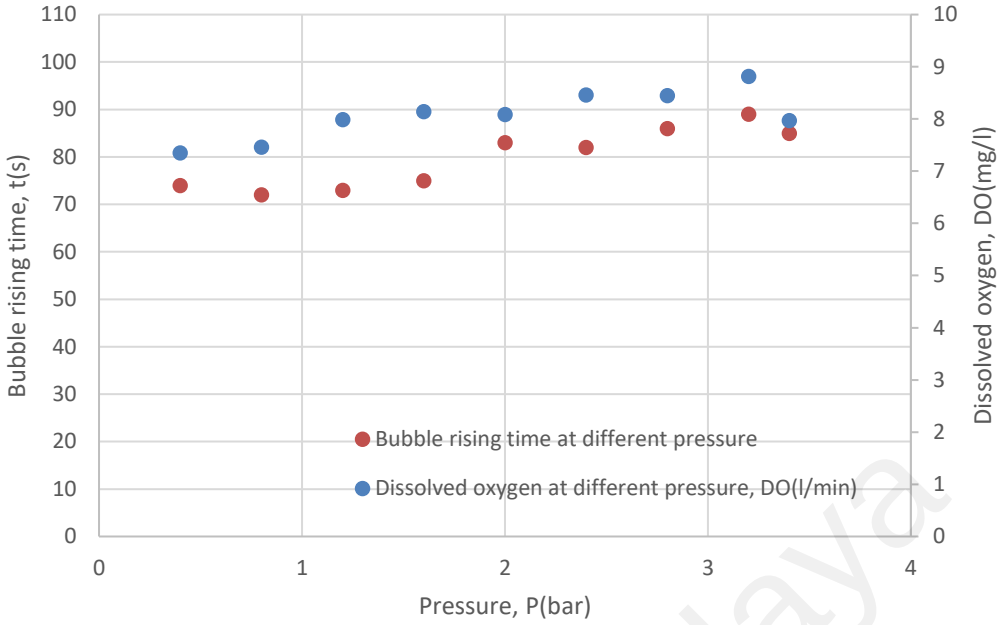

Figure 4.9: Bubble rising time and DO versus pressure for venturi and static mixer (case 2).

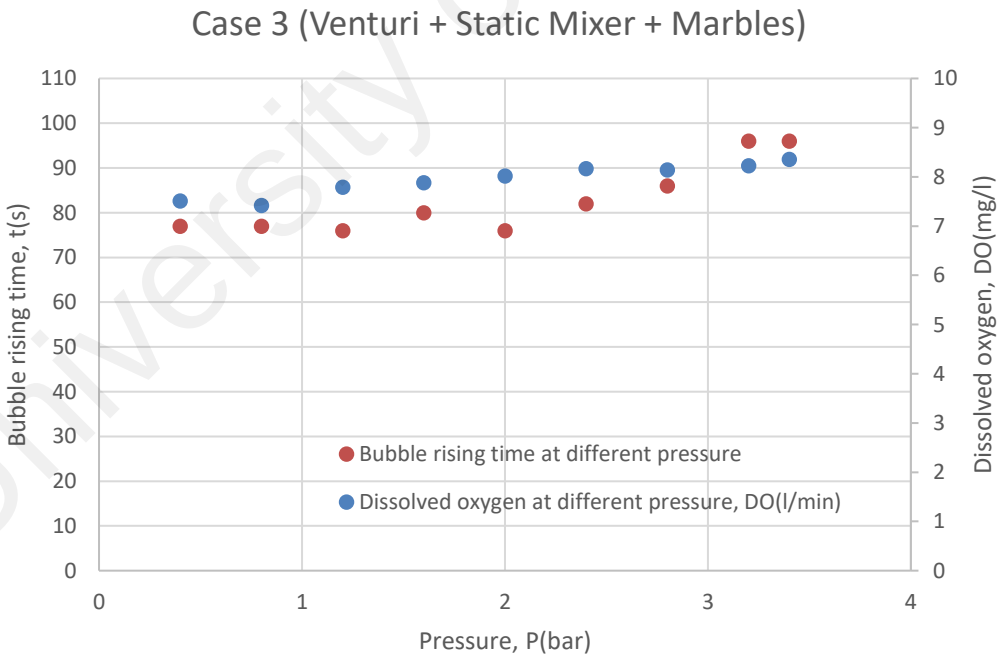

Figure 4.10: Bubble rising time and DO versus pressure for venturi, static mixer and single-phase marbles (case 3).

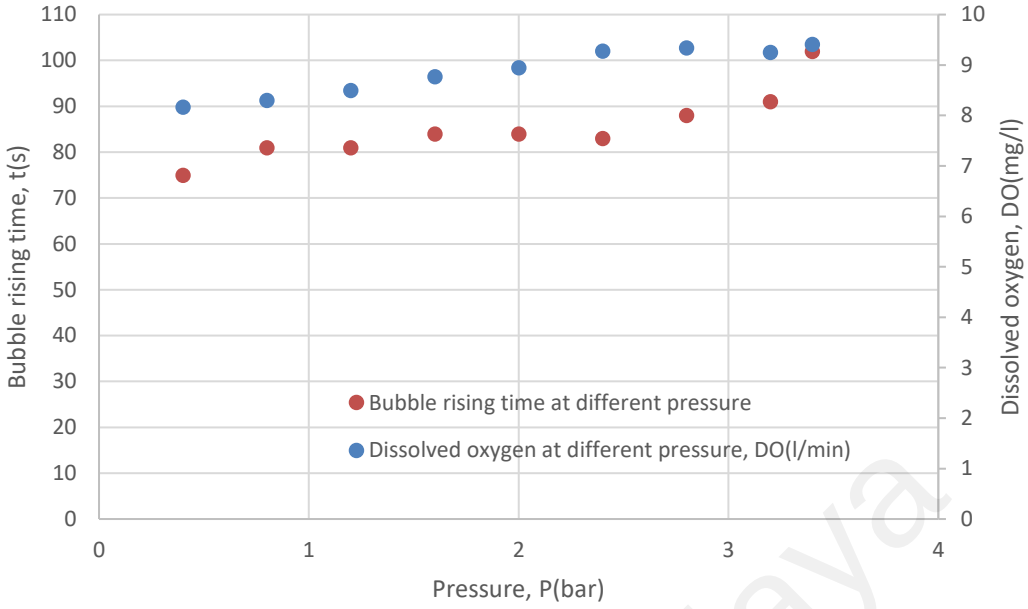

Figure 4.11: Bubble rising time and DO versus pressure for venturi, static mixer and two-phase marbles (case 4).

Moreover, the performance of DO and bubble rising time improved vastly after the implementation of static mixer. Similar trend was observed for case 2, case 3 and case 4 with increasing bubble rising time and DO as pressure increased. Increasing bubble rising time indicates a lower bubble rising velocity. As mentioned earlier, smaller bubbles possess low bubble rising velocity and they also have a larger surface to volume ratio compared to bubbles with larger diameter. According to Chisti (1989), the interfacial area of gas-liquid, a is expressed as a function of diameter of bubble, d_B (m) and gas holdup (ε), which is as shown below:

$$a = \frac{6\varepsilon}{d_B}$$

Chisti (1989) pointed out that the gas hold is depending on the dimeter of bubble at same inlet flow condition. In other words, higher gas holdup is generated by smaller diameter when greater interfacial area of gas-liquid is obtained, which means that a bubble with greater surface area to volume ratio is more beneficial for mass transfer of oxygen.

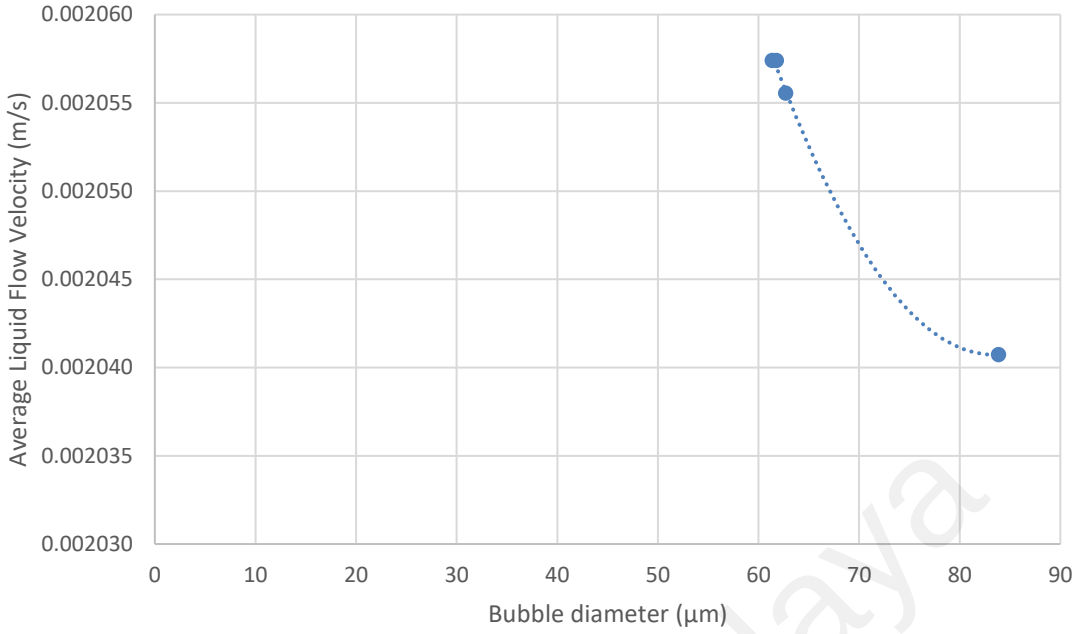

Figure 4.12: Average liquid flow velocity vs bubble diameter.

The average flow rates of the liquid were calculated and were plotted against the average bubble diameter and the data for 4 cases was presented in Figure 4.12. From the plotted graph, it can be observed that there was an increasing trend of bubble diameter from 61µm to 84 µm when the average liquid flow velocity dropped from 0.002057 m/s to 0.002041 m/s. This phenomenon can be linked to the buoyancy force bubbles with larger and smaller diameter. For bubble with larger diameter, it has a much lower drag force compared to buoyancy force, thus causing the momentum transfer to occur in a shorter period and resulted in lower liquid velocity. Furthermore, microbubbles are slower when they rise to the surface of water and they will experience longer period in momentum transfer and lesser momentum transfer. Therefore, microbubbles able to generate greater liquid circulation as they have longer time at dragging the liquid that moves along with them.

4.4 Effect of Air Intake Volume

The effect of air intake on dissolved oxygen (DO) and bubble diameter were plotted as shown in Figure 4.14 and Figure 4.15.

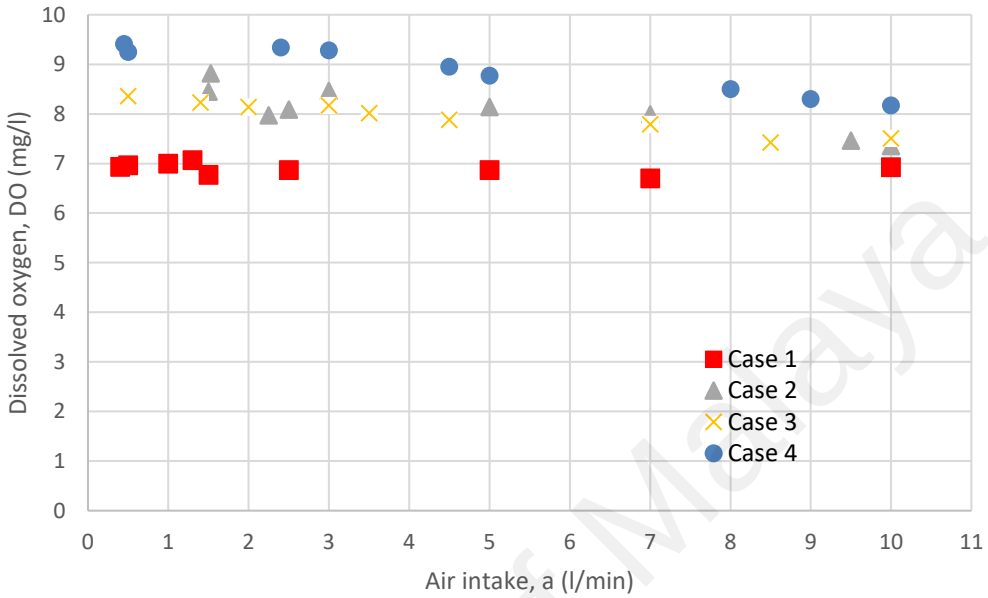

Figure 4.13: DO versus Air Intake

As shown in Figure 4.13, it can be observed that the dissolved oxygen produced venturi system was much lower than others and the average DO was around $7mg/l$. The DO trend started to change when static mixer was introduced into the venturi system. The DO value increased by around 13% when static mixer was used. However, the DO experienced slightly dropped when single-phase marbles were further installed into the system even the air intake was the same. This was due to the effect of temperature of water on the solubility of oxygen and the temperature of water obtained for case 3 was a little bit higher than case 2, where case 2 had average of 33.7 °C compared to case 3 which had average of 34.5 °C.

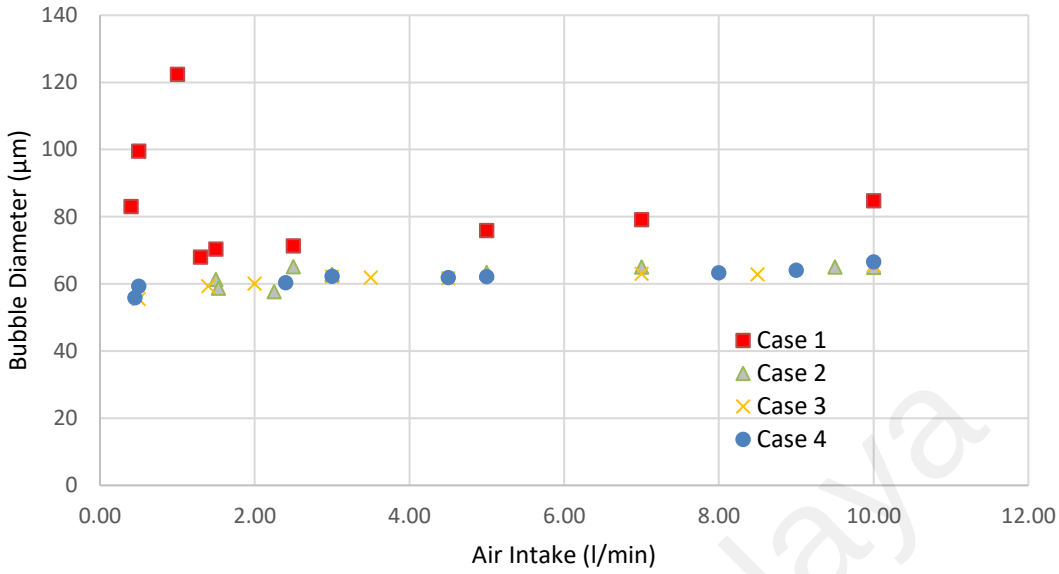

Figure 4.14: Bubble Diameter vs Air Intake.

Based on the graph plotted in Figure 4.14, it can be observed that the bubble diameter was affected by the air intake volume per minute. This phenomenon was obviously seen at case 1 where the bubble size changed substantially from 83μm to 122 μm as air flow rate increased from 0.40 l/min to 1.00 l/min. However, the bubble size reduced to 68 μm when the air flow rate was 1.3 l/min. When the air flow rate changed from 1.30 l/min to 10 l/min, 4 cases showed similar behavior where the bubble size increased slightly as air flow rate improved. This can be expected as an effect of Young-Laplace Law where the microbubble generation system encounters a pressure difference across water and air surface due to changes in air intake of volume. It is known that the curvature radius of bubble is inversely proportional to the pressure drop, therefore greater air flow rate will lead to a low acting pressure difference which results in large curvature radius.

Besides, the effect of air intake volume on the bubble size was also studied during the experiments. Ramakrishnan et al. (2001) stated that the air intake volume is a function of bubble size due to the surface tension effect. Take for example, the number of bubbles generated in an increasing manner as the air intake volume per minute increases. Those bubbles that formed previously influence the newly generated bubbles through the coalescence of old bubbles with new bubbles as the new bubbles emerge to the water surface and combines with the old bubbles. Coalescence takes place at the region adjacent to the nozzle surface when air flow rate increase and bigger bubble size will be obtained.

CHAPTER 5: CONCLUSION

5.1 Conclusions

In summary, the effect of different types of static mixer geometry on the quality of microbubble generation had been examined. A bench scale microbubble test experiment setup had been developed and effect of different dispersing elements on the quality of microbubbles by using different dispersing elements had been investigated as well.

The bubble rising time is a function of bubble diameter because tiny bubbles have low terminal rise velocity. In this research project, it was encountered that the diameter of bubbles decreased by 15% as the pressure of water increased from 0.4bar to 3.4bar. However, single-phase and two-phase marbles elements did not show any significant result in reducing bubble size. It can be said that multiple separation of dispersing elements did not contribute to bubble size reduction.

However, it was encountered that the dissolved oxygen (DO) of 2-phase marbles had improved by 7% to 15% compared to the case without 2-phase marbles installed into the system. For instance, at 3.4bar, DO recorded was 9.41 mg/l for 2-phase marbles compared to static mixer case where 8.82 mg/l was recorded.

In addition, the bubble diameter showed a linearly decreasing trend when the average liquid flow velocity increased from 0.002041 m/s to 0.002057m/s. So, the velocity of the liquid inside the pipeline system must be high enough to generate smaller size of bubbles because more drag force will be generated which will lead to high effective bubble shredding in the microbubble generation process.

5.2 Recommendations for Future Work

In future, it is recommended to conduct another study on the microbubble generation method which is by combining the ejecting method with static mixer to investigate the effect in terms of bubble size.

Also, it is also recommended to modify the test jig for the dispersing elements by changing the shape of the design from cylinder to cone shape and compare the differences. Other than that, the future study is suggested to focus on the bubble quality at air intake of value lower than 1litre/min.

REFERENCES

Agarwal, A., Ng, W. J., & Liu, Y. (2011). Principle and applications of microbubble and nanobubble technology for water treatment. *Chemosphere*, *84*(9), 1175–1180. https://doi.org/10.1016/j.chemosphere.2011.05.054

Ahmadi, R., Khodadadi, D. A., Abdollahy, M., & Fan, M. (2014). Nano-microbubble flotation of fine and ultrafine chalcopyrite particles. *International Journal of Mining Science and Technology*, *24*(4), 559–566. https://doi.org/10.1016/j.ijmst.2014.05.021

Aquacache. (n.d.). Dissolved oxygen air flotation D.A.F. Retrieved from http://aqua-cache.com/components/daf?fbclid=IwAR3OvpzAYTIksAXe4zmVfBSUfxh9CdCKpmAsiTU7NTBjeRVhzgYn2ic9ZLk

Brandner, P. A., Wright, G., Pearce, B., Goldsworthy, L., & Walker, G. J. (2010). An experimental investigation of microbubble generation in a confined turbulent jet. *17th Australasian Fluid Mechanics Conference 2010*, (December), 611–614.

Bruckner, M. Z. (n.d.). The Wrinkler Method- Measuring Dissovled Oxygen. Retrieved from https://serc.carleton.edu/microbelife/research_methods/environ_sampling/oxygen.html

Chen, Y. (2016). *Innovative Design for Vortex Micro-Nano Bubble generator Based on TRIZ*. (Icmit), 710–713. https://doi.org/10.2991/icmit-16.2016.127

Couto, H. J. B., Nunes, D. G., Neumann, R., & França, S. C. A. (2009). Micro-bubble size distribution measurements by laser diffraction technique. *Minerals Engineering*, *22*(4), 330–335. https://doi.org/10.1016/j.mineng.2008.09.006

Ebina, K., Shi, K., Hirao, M., Hashimoto, J., Kawato, Y., Kaneshiro, S., … Yoshikawa, H. (2013). Oxygen and Air Nanobubble Water Solution Promote the Growth of Plants, Fishes, and Mice. *PLoS ONE*, *8*(6), 2–8. https://doi.org/10.1371/journal.pone.0065339

FAO. (n.d.). National aquaculture sector overview. Retrieved from http://www.fao.org/fishery/countrysector/naso_malaysia/en#tcN70144

FONDRIEST. (n.d.). Dissovled Oxygen- What is dissolved Oxygen. Retrieved from https://www.fondriest.com/environmental-measurements/parameters/water-quality/dissolved-oxygen/

Fouan, D., Achaoui, Y., Payan, C., & Mensah, S. (2015). Experimental method for microbubbles dynamics monitoring and radius sizing. *Physics Procedia*, *70*, 1185–1189. https://doi.org/10.1016/j.phpro.2015.08.255

Fujiwara, A. (2006). Generating method of microbubbles by Venturi tube. *Eco Industry*, 22, 27-30 (in Japanese)

Han, M. Y., Kim, M. K., & Ahn, H. J. (2006). Effects of surface charge, micro-bubble size and particle size on removal efficiency of electro-flotation. *Water Science and Technology*, *53*(7), 127–132. https://doi.org/10.2166/wst.2006.216

Henderson. (n.d.). Airmaster venturi principle. Retrieved from http://www.hendersons.co.uk/wms/venturi_principle.html?fbclid=IwAR22RfilAuzfjwIqL9YuiYKanUDeQTSCUyn3z05y7gtHkHxI3zz8O8pWzow

Himuro, S. (2007).Characteristics of physical chemistry of microbubbles. *Chem. Eng.Jpn.*, *71,* 165-169 (in Japanese)

Kawamura, T., Kakugawa, A., & Kodama, Y. (2002). Controlling the size of microbubbles for drag reduction. *3rd Symposium on Smart Control of Turbulence*. Retrieved from http://www.nmri.go.jp/turbulence/PDF/symposium/FY2001/Kawamura.pdf

Kim, H. S., Lim, J. Y., Park, S. Y., & Kim, J. H. (2017). Effects on swirling chamber and breaker disk in pressurized-dissolution type micro-bubble generator. *KSCE Journal of Civil Engineering*, *21*(4), 1102–1106. https://doi.org/10.1007/s12205-016-1075-3

Kim, H. S., Lim, J. Y., Park, S. Y., & Kim, J. H. (2018). Effects of Distance of Breaker Disk on Performance of Ejector Type Microbubble Generator. *KSCE Journal of Civil Engineering*, *22*(4), 1096–1100. https://doi.org/10.1007/s12205-017-0208-7

Kim, S. J., Choi, J., Jeon, Y. T., Lee, I. chul, Won, C. H., & Chung, J. (2015). Microbubble-inducing characteristics depending on various nozzle and pressure in dissolved air flotation process. *KSCE Journal of Civil Engineering*, *19*(3), 558–563. https://doi.org/10.1007/s12205-013-0514-7

Kukizaki, M., & Goto, M. (2006). Size control of nanobubbles generated from Shirasu-porous-glass (SPG) membranes. *Journal of Membrane Science*, *281*(1–2), 386–396. https://doi.org/10.1016/j.memsci.2006.04.007

Kukizaki, M., & Goto, M. (2007). Spontatenous formation behavior of uniform-sized microbubbles from Shirasu-porous-glass (SPG) membranes in the absence of water-phase flow. *Journal of Membrane Science*, *296*(1–3), 174-181. https://doi.org/10.1016/j.memsci.2006.04.007

Lenntech. (n.d.). Static Mixers- Principle of Operation. Retrieved from https://www.lenntech.com/static-mixers.htm#Principles_of_operation/

Li, Pan. (2006). Development of Advanced Water Treatment Technology Using Microbubbles. *PhD Dissertation Keio University, Japan*, (October).

Li, Pan, Song, Y., & Yu, S. (2014). Removal of Microcystis aeruginosa using hydrodynamic cavitation: Performance and mechanisms. *Water Research*, *62*, 241–248. https://doi.org/10.1016/j.watres.2014.05.052

Li, Pan, & Tsuge, H. (2006). Water Treatment by Induced Air Flotation Using Microbubbles. *Journal of Chemical Engineering of Japan*, *39*(8), 896–903. https://doi.org/10.1252/jcej.39.896

Li, Peng, Zhang, H., Jiang, S., Qin, H., Ren, Y., & Sun, L. (2017). Microbubble Formation in a Co-flowing Liquid in a Microfluidic Chip. *Chemical Engineering and Technology*, *40*(8), 1512–1521. https://doi.org/10.1002/ceat.201700173

McCormick ME et al. (1973). Drag reduction of a submersible hull by electrolysis. *Naval Engineers Journal*, *85*(2), 11-16.

NASA. (n.d.). Drag of a sphere. Retrieved from https://www.grc.nasa.gov/www/k-12/airplane/dragsphere.html?fbclid=IwAR3I4ckkyNB8H2OiilTl0nj1wcLNPAjdD4JzYwMJd4smRCHJfKyx3vLl-OY

Noritake. (n.d.). What is a static mixer. Retrieved from https://www.noritake.co.jp/eng/products/support/detail/13/?fbclid=IwAR2hTBDY-LgIWIdZTdORRlbYPq55RnIf7_m1Itf62TXrmt0gZkbEf30FTVE

Ohnari, H. (2007). Today's subjects of microbubble technology. *Chem. Eng. Jpn*, *71*, 154-159. (in Japanese)

PUREBBLE. (n.d.). Frequent ask question..
Retrieved from
http://purebble.com/en/faq/

Sadatomi, M., Kawahara, A., Matsuura, H., & Shikatani, S. (2012). Micro-bubble generation rate and bubble dissolution rate into water by a simple multi-fluid mixer with orifice and porous tube. *Experimental Thermal and Fluid Science*, *41*, 23–30. https://doi.org/10.1016/j.expthermflusci.2012.03.002

Sadatomi, M., Kawahara, A., Matsuyama, F., & Kimura, T. (2007). An advanced microbubble generator and its application to a newly developed bubble-jet-type air-lift pump. *Multiphase Science and Technology*, *19*(4), 323–342. https://doi.org/10.1615/MultScienTechn.v19.i4.20

ScienceEncyclopedia. (n.d.). Fluid dyanamic- shape and drag.
Retrieved from
https://science.jrank.org/pages/2769/Fluid-Dynamics-Shape-drag.html?fbclid=IwAR3N9bEdxIsYDvREypR81j4L3k0tOmzA5S2IZj3UPs3gwdl7T57MUQ1Oo9w

Stamixco. (n.d.). Principle of operation of static mixers.
Retrieved from
http://www.stamixco-usa.com/principles-of-operation?fbclid=IwAR0T90htDwJN2druJ-o7MYXvmPaa8cq4O30oMHazb3IETOYeGU18hnDBKQs

Statiflo. (n.d.). Principle of operation of statiflo static mixer.
Retrieved from
https://www.statiflo.com/about-static-mixing/principles-of-operation/

Stride, E. (2009). Physical principles of microbubbles for ultrasound imaging and therapy. *Cerebrovascular Diseases*, *27*(SUPPL. 2), 1–13. https://doi.org/10.1159/000203122

Stride, E. P., & Coussios, C. C. (2010). Cavitation and contrast: The use of bubbles in ultrasound imaging and therapy. *Proceedings of the Institution of Mechanical Engineers, Part H: Journal of Engineering in Medicine*, *224*(2), 171–191. https://doi.org/10.1243/09544119JEIM622

Sumikura, M., Hidaka, M., Murakami, H., Nobutomo, Y., & Murakami, T. (2007). Ozone micro-bubble disinfection method for wastewater reuse system. *Water Science and Technology*, *56*(5), 53–61. https://doi.org/10.2166/wst.2007.556

TABEI, K., HARUYAMA, S., YAMAGUCHI, S., SHIRAI, H., & TAKAKUSAGI, F. (2007). Study of Micro Bubble Generation by a Swirl Jet. *Journal of Environment and Engineering*, *2*(1), 172–182. https://doi.org/10.1299/jee.2.172

Takahashi, M., Chiba, K., & Li, P. (2007). Free-radical generataion from collapsing microbubbles in the absence of a dynamic stimulus. *J.Phys. Chem. B, 111*, 1343-1347

Terasaka, K., Saito, J., Toda, Y., & Kobayashi, D. (2009). Micobubble generation using direct-contact condensation of mixed vapour. *Progress in Multiphase Flow Research, 4*, 103-110 (in Japanese)

Tesař, V. (2017). What can be done with microbubbles generated by a fluidic oscillator? (survey). *EPJ Web of Conferences*, *143*. https://doi.org/10.1051/epjconf/201714302129

Tsuge, H. (2015.). Micro- and Nanobubbles. *Pan Stanford Publishing Pte Ltd*.

Tsuge, H. (2004). *The Latest Technology on Microbubbles and Nanobubbles II*. 2nd ed. CMC Books Co., Japan. (in Japanese)

Tsuge, H., Li, P., & Hirofumi, O. (2004). Application of Induced Air Flotation on Water Treatment. *(86)*, 1–7. Retrieved from https://www.jstage.jst.go.jp/article/apcche/2004/0/2004_0_620/_pdf

Wu, C., Li, P., Xia, S., Wang, S., Wang, Y., Hu, J., … Yu, S. (2019). The role of interface in microbubble ozonation of aromatic compounds. *Chemosphere*, *220*, 1067–1074. https://doi.org/10.1016/j.chemosphere.2018.12.174

Zimmerman, W., Tesar, V., Butler, S., & Bandulasena, H. (2008). Microbubble Generation. *Recent Patents on Engineering*, *2*(1), 1–8. https://doi.org/10.2174/187221208783478598

911Metallurgist. (n.d.). Beaker Decantation Method: Classify Particles by Settling. Retrieved from https://www.911metallurgist.com/blog/beaker-decantation-method